NASA Contractor Report 202342

Probabilistic Mesomechanical Fatigue Model

Robert G. Tryon
Vanderbilt University
Nashville, Tennesseee

April 1997

Prepared for
Lewis Research Center
Under Grant NGT–51053

National Aeronautics and
Space Administration

ACKNOWLEDGMENTS

The author wishes to express his gratitude for the technical and financial support through NASA Graduate Students Research Program, NGT-51053, Lewis Research Center, Dr. C. C. Chamis, Technical Advisor.

TABLE OF CONTENTS

LIST OF FIGURES

LIST OF TABLES

CHAPTER I

INTRODUCTION

Ever increasing economic demands are requiring higher and higher reliability of structures and components. Human safety concerns require that the probability of failure be small for many structures. Small probabilities of failure can be assured by applying large safety factors based on previous experience. Safety factors can be expensive because the true safe life may be much greater than the life predicted using safety factors. Designing cost effective highly reliable structures requires the ability to accurately assess safe life.

If the uncertainty in structural loading and the uncertainty in structural response can be quantified, reliability methods developed in the past few years can be used to accurately estimate the safe life of structures. Tryon *et al.* [1] used probabilistic structural analysis methods to predict the reliability of a gas turbine rotor experiencing an in-service fatigue cracking problem. Variations in loading, temperatures, gas flow, and material properties were considered. The investigation showed that analytical and semi-analytical models such as structural finite elements and computational fluid dynamics are available to relate many of the primitive design variables to the fatigue response. A primary deficiency in fatigue reliability modeling revealed in the investigation was the lack of materials models which link the scatter in fatigue behavior to primitive variables.

The present study addresses the scatter in fatigue by investigating the variables responsible for the scatter and developing analytical and semi-analytical models to

quantitatively relate the variables to the response. For the purpose of this research, fatigue is defined as the entire range of damage accumulation sequences; from crack nucleation of the initially unflawed structure to final fast fracture.

The coefficient of variation (COV) of fatigue life tests range widely depending on the material alloy and load level. Even for well controlled laboratory test of annealed smooth specimens at room temperature, the COV varies from less than 10% [2] to over 500% [3] for different steel alloys. This indicates that the fatigue reliability experienced by components in the field may be substantially attributed to the material behavior.

Most crack nucleation models are empirically–based macrostructural models [4]. They reduce crack nucleation to simple parametric functions of macro-stress and macro-strain variables. As such, the macrostructural models assume the material to be homogeneous and isotropic. The models are necessarily approximate because they cannot represent the heterogeneous media in which the damage processes occur. In contrast to macrostructural models, micromechanical models establish material behavior based on the explicit response of the microelements, such as dislocations and slip planes. Micromechanics have successfully explained the qualitative behavior of crack initiation. However, a theoretical crack initiation model which explicitly relates the microstructure to the macroresponse has not been developed because too many complex micromechanical processes are operating simultaneously [5].

Statistical concepts have been used to develop empirical fatigue life models in which the independent variable (applied stress or strain) is considered deterministic and the dependent variable (life) is considered random [6]. The models do not account for the mechanisms that regulate fatigue damage and thus, the source of the scatter

is unknown and must be attributed to incomplete data and missing parameters. The models cannot be used to accurately describe materials and loading conditions that are not explicitly part of the data-based test program.

This study addresses the statistical aspects of fatigue using a fundamentally different approach. The fatigue mechanisms are considered and the independent variables, which include material variables that govern response, are recognized as random variables. The approach identifies the sources of uncertainty and quantitatively links the variation in the material microstructure to the scatter in the fatigue response.

The research is based on the concepts of probabilistic mesomechanics [7] which provides the relationships between the microstructural material properties and non-continuum mechanics [8]. In this research, the mesoelements are defined as the individual grains of a polycrystalline aggregate. Each grain is considered a single crystal with homogeneous (although not isotropic) properties. The properties are considered to vary from grain to grain. The macrostructure is modeled as an ensemble of grains. The material properties of the ensemble of grains is defined using the appropriate statistical distributions. Mesomechanical modeling is an approximation of the actual material because certain properties will vary within a grain. However, it is believed that mesomechanics is a better approximation of the true material characteristics than macromechanics.

Mesomechanics also recognizes the multiple stages of fatigue damage accumulation such as crack nucleation, small crack growth, and long crack growth. Each stage is driven by different mechanisms and must be distinctly modeled. The stages must be quantitatively linked because the crack grows successively from one stage to the next. In this research, a theoretical micromechanical model is used to determine the

number of cycles necessary to nucleate a crack in the individual grains. A combination of models based on empirical observations and theoretical micromechanics are used to determine the number of cycles necessary to grow the cracks from nucleation to the long crack regime. An empirically-based (Paris law) model is used to determine the number of cycles necessary for the crack to grow through the long crack regime to the critical crack size. Failure of the macrostructure is defined by the first crack to nucleate and grow beyond the critical crack size. The statistical distribution of fatigue life for the macrostructure is determined using Monte Carlo simulation methods. The probabilistic mesomechanical model provides a direct quantitative link between the variations in the material microstructure to the scatter in the fatigue behavior.

CHAPTER II

BACKGROUND

Various Stages of Fatigue

Current fatigue life prediction methods in metallic components consider three stages: crack initiation, long crack propagation, and final fracture. Long crack propagation and final fracture are the stages of damage accumulation that are well characterized using linear elastic or elastic-plastic fracture mechanics. Crack initiation is the early stage of damage accumulation where small cracks (cracks with depths less than several grain diameters) have been observed to deviate significantly from predicted long crack fracture mechanics behavior [9]. The deviation is attributed to the heterogeneous media in which small cracks evolve.

The crack initiation stage can be broken down into two phases: crack nucleation and small crack growth. Crack nucleation is the locally complex process of crack formation on the microstructural scale. Crack nucleation is characterized by smooth fracture surfaces at angles inclined to the loading direction. This type of failure is indicative of shear stress Mode II (sliding mode) fracture. Although loading has been shown to effect the nucleation size [10, 11], experimental evidence suggest that the nucleation size is on the order of the grain size [12, 13, 14].

Small crack growth is characterized by fracture surface striations perpendicular to the loading direction. This type of failure is indicative of tensile stress Mode I (opening mode) fracture. The behavior of small cracks tend to transition to linear or elastic-plastic fracture mechanics behavior when the crack depth reaches about ten

mean grain diameters [15]. Crack nucleation and small crack growth must be modeled separately because different mechanisms control each phase.

The relative importance of the crack nucleation stage on overall fatigue life depends on several factors. Materials which exhibit a strong preference for planar slip show a strong correlation between the crack causing final fracture and the earliest nucleated cracks [2]. Materials which prefer cross slip showed almost no correlation between the crack causing final fracture and the earliest nucleated cracks [2]. The relative importance of the crack nucleation may also depend on the loading condition. If the loading is relatively low (high cycle fatigue), the majority of life will be spent in the nucleation of a crack. If the loading is high (low cycle fatigue), cracks may nucleate early and spend the remainder of the fatigue life in the crack growth stages. However, high strength materials have been shown to spend the majority of fatigue life in the crack nucleation stage, even during low cycle fatigue [16].

Scatter in Fatigue Life

Sasaki et. al. [2] compare the variation in crack nucleation life of mild steel, pure copper, and stainless steel. They found that the COV clearly depends on the stacking fault energy denoted by Γ. Relatively low COV was found for mild steel, which has high Γ (wavy slip), and high COV was found for stainless steel, which has low Γ (planar slip). Copper, which has an intermediate Γ, was found to have a value of the COV between mild and stainless steel.

Figure 1 shows the relative scatter in the different stages of crack growth for sixteen mild steel specimens exposed to high cycle fatigue [17]. The specimens were shallow notched and tested in rotating bending. The cracks nucleated at a size roughly equal

to the mean grain size (0.07mm). The small crack regime for this data extends from the initiation event until the crack reaches about eight times the mean grain size (0.6mm). The long crack growth regime extends from 0.6mm to failure. Figure 1 illustrates the larger amount of scatter in the early stages of crack growth with relatively little scatter (similar slopes) in the large crack growth stage. The variation is attributed to the heterogeneous media in which small cracks evolve.

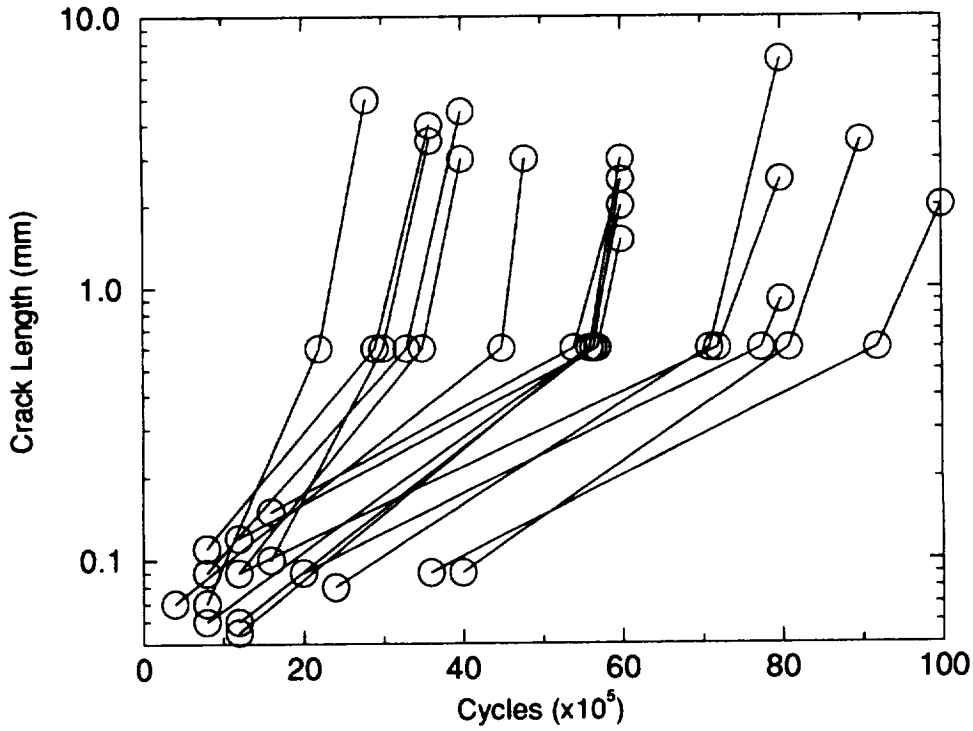

Figure 1: Crack growth curves for mild steel.

Table 1 shows the scatter factors for a NiCrMoV steel turbine rotor shaft material data found in the literature [18]. The specimens were shallow notched round bars tested in rotating bending low cycle fatigue. The values are for a 99.87% (3σ) reliability at 90% confidence level using the life reduction model found in [19], which assumes a lognormal life distribution. The behavior in Figure 1 and Table 1 is observed for different stresses amplitudes and materials [2, 17, 20, 21].

Failure definition	Number of samples	Mean life (cycles)	Scatter factor	-3σ life (cycles)
Nucleation	36	26,700	44.2	604
Small crack	36	52,400	15.5	3380
Final fracture	14	82,400	2.78	29,600

Table 1: Scatter factors for stainless steel in low cycle fatigue

The values in Table 1 show the importance of material response scatter. The scatter factors are life reduction factors for material response scatter only. They do not account for variations in loading, geometry, environment, temperature, or size effect. The potential for improved design through the reduction of material scatter is great. When you consider that fatigue is estimated to account for at least 90% of all service failures due to mechanical causes [22], understanding the statistical aspects of fatigue becomes paramount.

Limited experimental work has been performed with regard to the effect of microstructural variation on other aspects of material response. Gokhale and Rhines [23] prepared pure aluminum to give several grain size distributions with the same mean grain size but different variances. They found that the scatter in grain size played a primary role in controlling yield stress, ultimate tensile stress, reduction in area, and the area under the stress-strain curve. The parameters were much more sensitive to changes in the grain size variance than to changes in the mean grain size. This research emphasizes the importance of microstructural variation with regard to any type of plastic behavior which is likely to be important to crack initiation and growth kinetics.

Probabilistic Mesomechanics

Many material and structural design factors influence component reliability in terms of the defined durability problems. From a material performance standpoint, many of these factors are at work in the durability "size effect." The size effect was first reported by Peterson [24] when he noticed that the mean fatigue life and variation in fatigue life were a function of the stressed area. The size effect has a fundamental role in controlling reliability because damage accumulation starts on a small scale and grows through various characteristic sizes, each with its own geometric complexities, constitutive laws, and heterogeneities. Fatigue behavior cannot be fully understood and predicted without obtaining information about each of the characteristic sizes, or what can be called mesodomains [8]. Nested models can link each of the mesodomains to determine the response of the macrodomain [25].

The concepts of mesomechanics can be used to explicitly examine each of the characteristic sizes or mesodomains. For example, a fleet of simple polycrystalline metallic components may be divided into six mesodomains as shown in Table 2. At each level, heterogeneities can be introduced from various sources and fatigue damage can accumulate via various mechanisms.

The true primary mesodomain is below the dislocation level. The most primitive variables controlling fatigue may be at the atomic level. Modeling at such levels is not yet possible and is not required for the purposes of the present study. The slip process, which takes place on slip steps typically $0.1\mu m$ wide, is of continuum scale with respect to the atomic size of $0.5nm$ [26]. The smallest practical mesodomain depends on the material, loading, and available information gathering techniques. The research has focused on the use of slip band models from the sub-grain mesodomain, together with

Mesodomain	Sources of variation	Damage accumulation mechanisms
dislocation level	vacancies, interstitials	dislocation pile-up
sub-grain level	slip bands, micro-voids, second phase particles	slip band decohesion
grain level	crystallographic orientation, twins, inclusions	crack nucleation
specimen level	surface finish, cracks, notches	small crack growth
component level	cracks, notches, processing, geometry, machining	large crack growth, multiple cracks
fleet level	heat treatment, service duty, applications	NDE inspection screening, life distributions

Table 2: Mesodomains for a simple component

probabilistic variables being defined at the grain size mesodomain. These models are used to predict behavior for the specimen mesodomain.

The specimen level is an artificial mesodomain because there are no specimens in the fleet. Specimens are generally prepared so as to limit the introduction of heterogeneities. However, the bulk of the information used in design is usually gathered from specimen testing, so it is important to understand the characteristics of this level. Specimen testing can identify scale effects, defect origins, and processing influences on crack initiation.

A large component such as an aeroengine fan blade will have several mesodomains between the grain size and the component level. The airfoil and the dovetail would be two component-scale mesodomains. Properties such as the grain size, material properties, and surface finish are different in these two mesodomains. The delineation of the mesodomains is specific to the material, geometry, loading, and failure mode.

The overall fatigue response at the fleet level is predicted by nesting the individual

mesoscale models. The lowest level model uses the appropriate mesoscale parameters to determine the initial state of the next level. This level uses the results from the previous level along with the appropriate parameters to determine the initial state of the next level and so on. Through the use of nested models, fleet reliability can be linked to the heterogeneities at each mesodomain. Additionally, by modeling each level of the fatigue process individually, and rigorously linking the levels, various size effects are included.

Tryon and Cruse [27] use probabilistic mesomechanics to investigate the scatter in fatigue response. They consider two mesodomains: crack nucleation and long crack growth. The random variables considered, which apply only to the crack nucleation mesodomain, were: grain size and grain orientation.

The probabilistic mesomechanical model predicted some of the trends in observed fatigue behavior.

1. Both normal and lognormal distributions adequately described specimen fatigue life.

2. The failure causing cracks nucleated in the large grains.

3. The relative mean life of different size specimens agreed with size effect observations.

4. High strength alloys have more scatter in fatigue life then low strength alloys.

However, there were several discrepancies between the model predictions and experimental observations.

1. Predicted scatter was not a function of the applied stress.

2. No scatter was predicted in the endurance strength.

The discrepancy between the model predictions and the experimental observations was attributed to the fact that the model does not account for the scatter in small crack growth and the frictional stress was considered deterministic. In the current study, a small crack growth model is developed and the grain to grain variation in frictional stress is included.

CHAPTER III

CRACK NUCLEATION

Micromechanics of Crack Nucleation

Fatigue crack nucleation is a complex and obscure process. The mechanisms for crack nucleation change with material, loading, temperature, and environment. One overriding observation is that cracks tend to nucleate near the free surface. For many loading conditions, the highest loads are at the surface. But even when the nominal stress is constant throughout, cracks tend to nucleate at the surface because deformation of each grain is allowed to concentrate on a preferred crystallographic plane. In the interior, deformation on a single crystallographic plane is hampered by the constraints of the surrounding grains.

Experimental evidence clearly shows that defects in the material can cause fatigue crack nucleation by acting as stress concentrations and the cracks tend to nucleate along the preferred slip plane [28]. Examples of defects include surface pores, ceramics inclusions, second phase particles, and microcracks. The fatigue resistance of many alloys has been improved by decreasing the size and number of defects. However, slip band decohesion also causes crack nucleation even when no apparent defect is present. The surface grains must be favorably oriented for slip band decohesion to occur, but not all favorably oriented grains have cracks. Slip along preferred planes plays an important role in crack nucleation.

When annealed metals are exposed to cyclic loading, they strain harden. Strain hardening is one of the earliest mechanical responses to fatigue. Initial hardening is

rapid and controlled by multiplication of dislocations in the atomic lattice. When the material is first cycled, dislocations glide freely to accommodate large plastic strains. Eventually, the dislocations interact and start to create a substructure of pinned dislocations [29].

The substructure consist of veins for low stain amplitude and cells for higher strain amplitudes [30]. The veins and cell walls consist of high dislocation density while the volume between the veins and cell walls has a much lower dislocation density. The dislocations can only glide freely in the volume of low density. As the substructure develops, hardening will result because the increased interaction of dislocations constrain their movement. If the cyclic strain amplitude is increased, the cell size decreases which reduces the volume between cells, and hardening continues. Fine slip lines appear on the surface as the dislocation density increases [31].

The rate of hardening gradually decreases until the flow stress becomes constant. The dislocation substructure is saturated and can no longer accommodate strain. Saturation is accompanied by the formation of coarse slip bands which roughen the surface of the grain with extrusions and intrusions. If the surface is polished, small vacancy pits are found in the slip bands. If the specimen is again cycled, the same slip bands roughen the surface. These bands are referred to as persistent slip bands [31].

The persistent slip bands have a distinctive substructure of walls of high dislocation density [32]. The walls are perpendicular to the primary slip direction and stretch across the thickness of the band. The distance between the walls is fairly constant. This substructure is often referred to as a ladder structure [33].

Slip band behavior is not well understood and many different theories exist to explain how the bands accommodate strain [32, 33, 34, 35]. But it is recognized that

the strain is localized in the persistent slip bands and very little strain is accommodated by the volume of material between slip bands. Upon further cycling, cracks form in the persistent slip bands. The cracks are believed to be the combined result of vacancy creation, repulsive dislocation stresses, and surface roughening stress concentrations. Experimental evidence show that if the strain amplitude is lower than the saturation point, the strain is accommodated by fine slip associated with pre-saturation dislocation substructure and no cracking takes place [36]. Thus, persistent slip bands are essential to fatigue damage and must be addressed by crack nucleation models.

There are two fundamentally different types of slip-band-induced crack nucleation. One is Forsyth's well known Stage I crack nucleation in which a very small crack (much smaller than the grains size) nucleates along the slip plane very early in life. A crack is evident from crack opening displacement when a static load is applied [9]. The size of the plastic zone is relatively small, being equal to or less than the crack size [37]. The crack propagates in Mode II until it reaches an obstacle, often the grain boundary. This type of crack nucleation has been observed in age hardened aluminum [9] and alloy single crystals [31]. (Many of Forsyth's observations concerned single crystals.) Elastic-plastic crack growth models have been successful in modeling the mean behavior of such alloys down to a very small crack size [38].

The more prevalent though less recognized slip band induced crack nucleation is sudden crack nucleation. In sudden crack nucleation, a slip band which stretches across the grain forms very early in life but no crack is formed. The lack of a crack is evident from no crack opening displacement when a static load is applied [9]. The slip band is not associated with crack beneath the surface [35, 39]. Upon continued

cycling, the slip band is blocked by the grain boundary and does not grow in length. However, the depth and the width of the slip band increase slightly until suddenly a crack is form. This slip band crack nucleation behavior is observed in many alloys including steel, aluminum, and brass [9, 17, 40].

The crack nucleation model developed in this study addresses sudden crack nucleation. However, the small crack growth model presented in Chapter IV is applicable to Stage I crack nucleation.

Micromechanical Crack Nucleation Models

Models used in the research must have two attributes. They must be quantitative with regards to the number of cycles needed to produce a crack to a specific size if they are to be used for life-time predictions. The models must also be able to address the microstructural parameters in order to provide a physical link between the microstructure and the fatigue behavior. Although the literature contains numerous expressions for modeling the propagation rate of fatigue cracks as discussed later, only a limited number of analytical crack nucleation models exist. Most all of these models use dislocation theory [41] to model fatigue damage accumulation as the build up of a continuous array of dislocations [42].

Microstructural models which predict crack nucleation life and crack nucleation size have been proposed independently by Tanaka and Mura [34] and Chang *et al.* [43]. Both of these models predict damage accumulation through irreversible dislocation pile-up at microstructural obstacles. Cracks nucleate when a critical strain energy is exceeded. These models have been modified to include a wide variety of crack nucleation mechanisms including:

- slip band cracking within a grain [34]

- grain boundary cracking [44]

- matrix/inclusion interface cracking [44]

- cracks emanating from inclusions [34, 43]

- cracks emanating from notches [45]

The models have been modified to account for partial reversibility and random load amplitude [46].

The models are consistent with the Coffin-Manson relationship for fatigue crack initiation [44, 47], the Petch equation for the grain size dependency of the fatigue strength [44] and the Palmgren–Miner law of damage accumulation for variable amplitude loads.

The Tanaka and Mura Model

The crack nucleation model used in this study is based on one proposed by Tanaka and Mura [34] in which the forward and reverse plastic flow within the persistent slip band of a surface grain is related to the creation of dislocations of opposite signs on closely spaced planes. This model is applicable to metallic components for which crack nucleation takes place by transgranular shear stress fracture and is outlined below.

As a load greater than the local yield stress is applied to grain with diameter d, dislocations are generated and move along the slip plane as shown in Fig. 2. The dislocations pile up at the grain boundary which acts as an obstacle to dislocation

movement. The dislocation movement is assumed to be irreversible such that when the reverse load is applied, dislocations of the opposite sign pile up on a closely spaced plane. Since the residual load from the back stress of the positive dislocations act in the same direction as the reverse applied load, unloading will cause negative dislocation movement. During each of the subsequent load cycles, the number of dislocations monotonically increase.

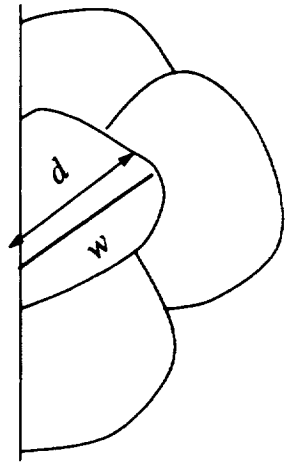

Figure 2: Slip bands interacting with the grain boundary.

On the first loading, the equilibrium condition can be expressed as

$$\tau_1^D + (\tau_1 - k) = 0 \tag{1}$$

where k is the frictional stress which must be overcome to move dislocations, τ_1 is the applied shear stress (τ_1 must be greater than k for damage to accumulation to occur), and τ_1^D is the back stress caused by the dislocations. If the dislocation density $D_1(x)$ along the slip plane is assumed to be continuous [42]

$$\tau_1^D = A \int_{-r}^{r} \frac{D_1(x')}{x - x'} dx' \tag{2}$$

$$A = \begin{cases} G/2\pi(1-\nu) & \text{for edge dislocations} \\ G/2\pi & \text{for screw dislocations} \end{cases}$$

where r is the grain radius, G is the shear modulus and ν is Poisson's ratio. Substituting Eq. 2 into Eq. 1 creates a singular integral equation which is solved for $D_1(x)$ using the inversion formula of Muskhelishvili [41, 48] for unbounded dislocation density at the grain boundary

$$D_1(x) = \frac{(\tau_1 - k)x}{\pi A\sqrt{r^2 - x^2}} \tag{3}$$

The incremental increase of dislocation density $\Delta D(x)$ with each load cycle is

$$\Delta D_1(x) = \frac{(\Delta\tau_1 - 2k)x}{\pi A\sqrt{r^2 - x^2}} \tag{4}$$

The slip displacement $\phi(x)$ due to the increment $\Delta D(x)$ is

$$\phi(x) = \int_x^r \Delta D(x)dx \tag{5}$$

The plastic strain increment $\Delta\gamma$ is

$$\Delta\gamma = \int_{-r}^{r} \phi(x)dx = \frac{(\Delta\tau - 2k)r^2}{2A} \tag{6}$$

such that the constitutive equation is

$$\gamma = \frac{(\tau - k)r^2}{2A} \tag{7}$$

which describes the stress-strain hysteresis loop in Fig. 3.

During the first forward loading of stress τ_1, the material hardens for any stress above k. (See Fig. 3.) On reverse loading to τ_2, the path ABC is followed. On subsequent forward loading, the path CDA is followed. The amount of plastic strain

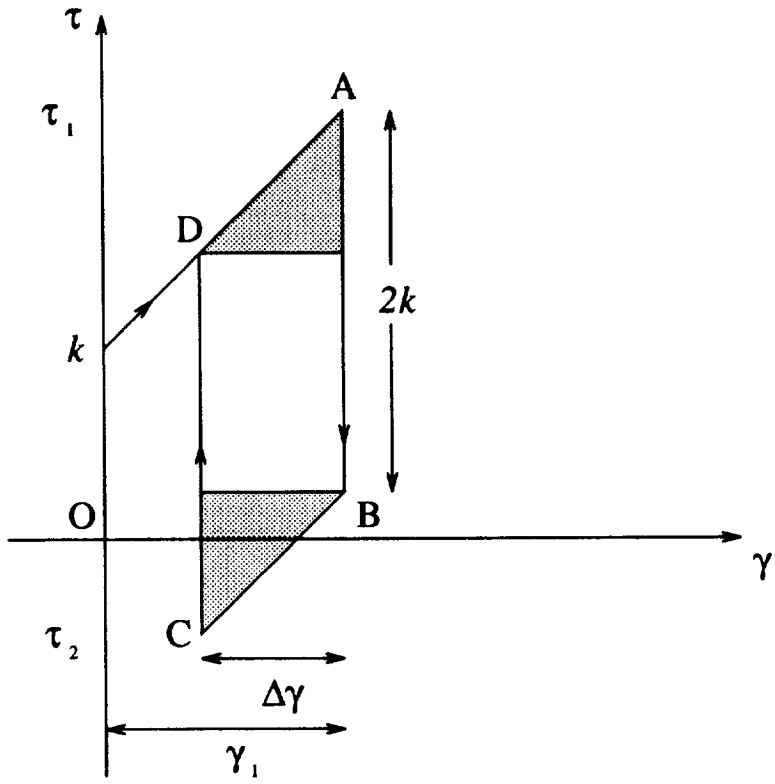

Figure 3: Stress-strain hysteresis loop.

increment is a linear function of $(\tau - k)$. The dislocation strain energy is the same for forward and reverse loading except the first loading. The incremental stored dislocation strain energy ΔU corresponds to the shaded area of Fig. 3.

$$\Delta U = \Delta\gamma(\Delta\tau - 2k) \tag{8}$$

The energy associated with the unshaded area of Fig. 3 is the dissipated work against the frictional stress k. Crack nucleation takes place when the total stored energy after N_n cycles is equal to the fracture energy of the grain.

$$N_n \Delta U = 2rW_s \tag{9}$$

$$N_n = \frac{4GW_s}{(\Delta\tau - 2k)^2\pi(1-\nu)d} \tag{10}$$

where d is the grain diameter and W_s is the specific fracture energy per unit area.

The probabilistic mesomechanical fatigue model calculates the crack nucleation life using Eq. 10 in a slightly modified form. The modification, discussed in Chapter VI, is that $\Delta\tau$ is replace with $\Delta\sigma/M$ where $\Delta\sigma$ is the applied axial stress and M is the grain orientation factor.

The model has several assumptions and limitations.

1. *The grain is homogeneous.* The dislocations are free to move to the grain boundaries i.e., no subgrain structure exists to pin or disrupt dislocation movement. Although the grain is homogeneous it is not isotropic.

2. *Damage accumulates on a single planar slip system.* In general, grains within a polycrystalline aggregate are not free to deform but are constrained by neighboring grains. Crack nucleation takes place on the surface grains which are not as constrained as grains embedded in the interior. Surface grain are able to accommodate more strain on the primary slip system [49]. The model can only be directly used on alloys that show planar slip.

3. *The crack nucleation size is equal to the grain size.* Although loading has been shown to effect the nucleation size (the crack size at Mode II to Mode I transition) [10, 11], experimental evidence suggest that the nucleation size is on the order of the grain size [12, 13, 14].

4. *The dislocation movement is irreversible and dipoles pile-up monotonically at the grain boundaries.* It is reasonable to expect some of the dislocations to

move back into the interior of the grain upon reverse loading or be annihilated by back stresses. Theoretical investigations on how to account for the partial reversibility of slip band formation have been inconclusive [46, 50, 51]. However, there is experimental evidence that this reverse movement is small [34].

5. *The number of cycles to saturation are negligible.* This assumption is reasonable for many materials under certain loading conditions [14, 31].

Equation 10 is necessarily a simplification of the complex phenomenon of slip band cracking. It does not directly address the effect of vacancy creation or the stress concentration of the surface roughening. However, the model is attractive because the fatigue life is inversely proportional to the square of the plastic strain amplitude which is in agreement with the Coffin-Manson empirical equation for fatigue. Equation 10 can be rewritten as

$$\Delta\tau = 2k + \left(\frac{4GW_s}{\pi(1-\nu)}\right)^{\frac{1}{2}} d^{-\frac{1}{2}}$$

which is in the form of the Hall-Petch equation for the dependence of fatigue strength on grain size.

CHAPTER IV

SMALL CRACK GROWTH

The behavior of small cracks differs from the behavior of long cracks. Long crack behavior can be predicted using conventional continuum based LEFM techniques. Small crack growth rates vary widely, from several orders of magnitude greater than that predicted by continuum based ΔK to complete arrest. A small crack can be thought of as a crack with a size on the order of the microstructure. The anomalous growth of small cracks has been attributed to two competing factors: high growth rates due to lack of closure and plane stress at the surface and growth retardation due to microstructural obstacles [52].

Similarity in the fracture surface of small and long cracks indicate a common Mode I cracking mechanism [53]. The anomaly in growth rates must be caused by a difference in the crack driving force [54]. The difference in driving force could be caused by several factors. The plasticity of a small crack is different than that of a long crack because the plastic zone is in one grain which displays anisotropy [55]. The plasticity tends to concentrate along slip planes causing the crack to grow along the slip plane. The slip plane is not necessarily perpendicular to the applied stress field. This could cause the crack to grow in multiple modes. So, when the crack is small, the crack can grow more easily along a preferred plane. Large cracks must grow simultaneously in many grains, some of which will not have a preferred plane oriented in the direction of the crack.

The closure mechanism also seems to be fundamentally different for long and

small cracks [56]. Long cracks tend to have a closure stress which must be overcome to open the crack tip. Small cracks are more likely to be open at zero load [57, 58]. The residual stresses at the crack tip that effect closure may be different for small cracks due to the difference in plasticity. The planar growth of small cracks causes the crack surface to be smoother than long cracks. The limited roughness of the small crack surface topography allows for reduced crack tip shielding [56, 59].

Crack Tip Opening Displacement

The experimentally observable parameter that has been correlated to the varying small crack growth rate is the crack opening displacement (COD) [37]

$$\frac{da}{dN} = C'(\Delta \mathrm{COD})^{n'} \tag{11}$$

The COD is measure of the amount of damage associated with the crack tip. The larger the COD the higher the crack growth rate. This phenomenon was first observed by Laird and Smith [60] and has been well established in long crack growth [61, 62]. The exponent n' has been found to have a value near unity when the COD is replaced by crack tip opening displacement (CTOD)

$$\frac{da}{dN} = C'(\Delta \phi^t) \tag{12}$$

where the CTOD, denoted by ϕ^t, is measured at the location of crack extension for the previous cycle. The direct proportionality of Eq. 12 has been observed in small crack growth of aluminum, nickel, and titanium alloys [63]. Equation 12 has also been shown to correlate the behavior between small and long crack growth [64]. Nisitani and Takao [9] showed that small crack arrest could be associated with no CTOD. Tanaka *et al.* showed that regressing data to Eq. 11 showed much less scatter than

exponential models based on ΔK or ΔJ. Also, developing models for three different materials; copper, mild steel and stainless steel, produced very similar values for C' and n'. (The exponent $n'$was not unity because the COD measurements were made on the specimen surface at the center of the crack.) It appears as though the relationship between da/dN and $\Delta\phi^t$ is more of an intrinsic material behavior than models based on ΔK or ΔJ.

Determining C' for small crack growth has been performed through direct microscopic observations [9]. However, there has been limited success in using ΔK or ΔJ data to determine C'.

CTOD can be shown to be related to the J integral through

$$\phi^t = \alpha \frac{J}{\sigma_0} \tag{13}$$

where σ_0 is the bulk yield strength and α is nearly unity [65]. Assuming elastic perfectly plastic behavior, CTOD can be related to K through

$$\phi^t = \frac{2K^2}{\pi\sigma_0\nu} \tag{14}$$

where ν is Poisson's ratio. Combining Eqs. 12 and 14

$$\frac{da}{dN} = \frac{C'\Delta K^2}{2\pi\sigma_0\nu} \tag{15}$$

which is the form of a second-order Paris equation. Determining C' using da/dN vs. ΔK data is straight forward for alloys that are governed by a second-order Paris relationship. Donahue *et al.* [66] have compiled an extensive list of data that fit a second-order Paris equation. They find a C' value of about 0.1 fits most of the data. However, in general the Paris exponent is not expected to be 2.

It is interesting to note that McEvely [67] presents data form several sources which shows that a well defined region of constant slope is seldom found in the Paris fit. The slope was found to vary with ΔK and have a value of 2 at low ΔK (the region of interest in the present study) and increase at higher ΔK. Also, there has been some success [68] with correlating data to

$$\frac{da}{dN} = C''\Delta K_{eff}^2 \tag{16}$$

where ΔK_{eff} is the effective ΔK which is the applied ΔK minus the ΔK when the crack first opens. However, the measurement of ΔK_{eff} still requires direct observation.

The relationship in Eq. 12 is assumed to be valid and will be used in the present study.

Small Crack Growth Models

Two basic approaches have been used to model small crack growth behavior: modify a continuum mechanics based stress intensity factor, K, to account for the microstructural heterogeneity or, explicitly model the damage ahead of the crack tip using dislocation theory. Hobson [69] presented a simple continuum based model in which the crack growth rate is related to the distance between the crack tip and the nearest grain boundary. All of the model parameters are determined by fitting the model to experimental data. Chan *et al.* [37] modifies K to account for grain size and orientation using a simple analytical approach. Chan *et al.* [70] uses a more rigorous analytical approach to modify K for microstructural effects and large scale yielding. They introduce the concept of microstructural dissimilitude which accounts for the

fact that small cracks actually lie in relatively few grains. Similitude can be assumed when the crack front interrogates enough grains such that the material properties averaged along the crack front have the same value as the bulk material properties. When the crack front interrogates relatively few grains, the average material properties at the crack front can vary significantly from the bulk properties, hence, microstructural dissimilitude. The number of grains interrogated by the crack front necessary to assume similitude depends on the amount of scatter in the local material properties. Also, by using an equivalent properties model that effectively averages the microstructural environment interrogated by the two dimensional crack front, Chan *et al.* were able to reduce small crack growth to a one dimensional problem.

Gerberich *et al.* [71] used a modified continuum approach to address the semi-cohesive zone associated with selective cleavage in the microstructure at the crack tip for Ti-6Al-4V. Using this model, they were able to predict the mean grain size effect on threshold for titanium alloys.

Bilby and his coworkers [42, 72] described the damage ahead of the crack tip using the theory of continuous dislocations. The models are equivalent to the Dugdale [73] model found by a different method. Weertman [74] used Bilby's model to develop a fatigue crack growth law and later used dislocation theory to developed a K for short cracks [75].

Several researches have extended Bilby's model to account for microstructural effects. Taira *et al.* [76] obtained a model for a crack tip slip band blocked by a grain boundary. Tanaka *et al.* [77] extended Taira's model to slip band propagation through grain boundaries. The CTOD predicted by the model was found to be equivalent to that predicted by both Morris *et al.* [78] and de los Rios *et al.* [79]. Navarro *et al.* [80]

used an equivalent model to Tanaka's to describe small and short crack growth. The models predicted the bounds on the variation in small crack growth.

Many statistical and probabilistic crack growth models can be found in the literature. The Markov-based models [81] describe the crack growth rate scatter as a process in which the amount of crack extension for each cycle is a random function. The Paris-based models [82] describe the crack growth rate scatter by allowing the material property parameters to be random. A common feature of these models is that the random nature of the crack growth is not related to microstructural variables. Thus, these models are not useful in understanding small crack growth behavior.

Limited work has been reported on models which directly addresses the statistical aspects of small crack growth. Morris *et al.* [83] used Monte Carlo simulation to model the crack initiation behavior of aluminum smooth round bars. They used the crack nucleation model of Chang *et al.* [43] described in Chapter III and a modified, continuum-based-K, small crack growth model. The random variables included crystallographic orientation, grain diameter, inclusion diameter, and an experimentally determined material parameter associated with the fracture strength of the inclusion. The statistical distributions of the random variables were not discussed. The predicted results compared favorably to the experimental observations. Tanaka *et al.* [84] used Monte Carlo simulation to predict the general behavior of small crack growth. They used the small crack growth model of Tanaka *et al.* [77]. The random variables included grain size, grain frictional stress, and an independent grain boundary strength. A two-parameter Weibull distribution was assumed for all of the random variables. They extended the model to include two-phase materials. Trends predicted by the model compared favorably with general trends observed in small

crack growth behavior.

A Model Based on Continuously Distributed Dislocations

The model chosen for the small crack growth life calculations in the probabilistic mesomechanical fatigue model follows the approach used by Tanaka *et al.* [77]. The approach derives from the model presented in Chapter III, thus allowing consistency in the theory, mathematical equations, and governing variables between the crack nucleation and small crack growth phases. The approach is outlined below for Mode II (sliding) crack growth. The solution for Mode I (tensile) crack growth is obtained through the simple transformations discussed at the end of the section.

Assume a crack has length a and the crack tip lies within a grain as shown in Fig. 4. As load is applied, dislocations are emitted from the crack tip creating a slip band with dislocation density $D(x) > 0$ as represented by the length ω in Fig. 4. For low stress ($\tau < k$) and the slip band tip far from the gain boundary ($c < d$) a condition called *equilibrium slip band* exist.

The solution for the equilibrium slip band was obtained by Bilby *et al.* [72]. The equilibrium condition can be expressed as

$$\tau^D + \tau^0 = 0$$

$$\tau^D = A \int_{-c}^{c} \frac{D(x')}{x - x'} dx' \tag{17}$$

$$\tau^0 = \begin{cases} \tau & x < a \\ \tau - k_1 & a < x < c \end{cases}$$

where τ is the resolved applied shear stress and k_1 is the friction stress of the grain in which the crack tip and slip band lie. The size of the slip band ω is determined

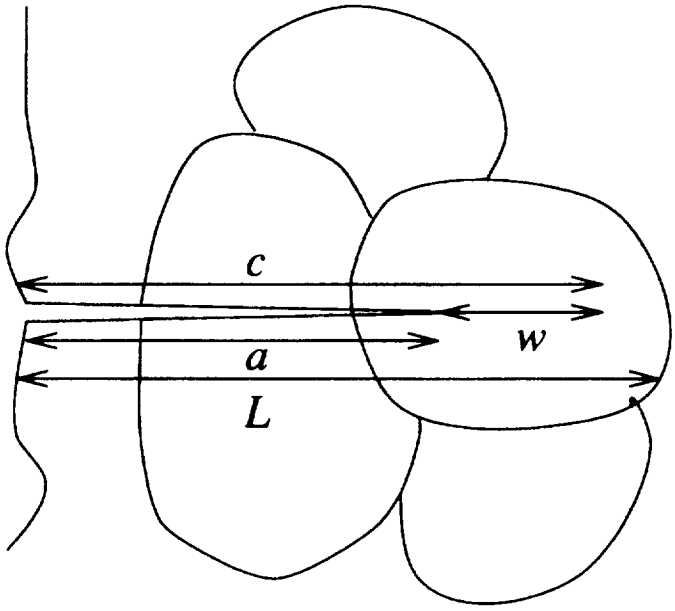

Figure 4: Crack tip in grain.

from the condition of vanishing dislocation density at the slip band tip.

$$\omega = c - a \tag{18}$$

$$\frac{a}{c} = \cos\left(\frac{\pi\tau}{2k_1}\right) \tag{19}$$

The dislocation density $D(x)$ is obtained by solving the singular integral Eq 17 using the inversion formula of Muskhelishvili [41, 48] for unbounded dislocation density at the crack tip.

$$D(x) = \frac{k_1}{\pi^2 A} f(x;c,a) \tag{20}$$

$$f(x;c,a) = \ln\left|\frac{x\sqrt{c^2-a^2}+a\sqrt{c^2-x^2}}{x\sqrt{c^2-a^2}-a\sqrt{c^2-x^2}}\right| \tag{21}$$

The crack tip sliding displacement (CTSD) is

$$\phi^t = \frac{2k_1 a}{\pi^2 A}\ln\frac{c}{a} \tag{22}$$

$$= \frac{2k_1 a}{\pi^2 A} \ln\left[\sec\left(\frac{\pi\tau}{2k_1}\right)\right] \tag{23}$$

As the crack grows, the tip of the slip band will eventually be blocked at the grain boundary. This condition is called the *blocked slip band.*

The solution for the blocked slip band was obtained by Taira *et al.* [76]. The size of the slip band is simply

$$\omega = c - a \tag{24}$$

$$c = L \tag{25}$$

The dislocation density $D(x)$ is obtained by solving the singular integral Eq 17 using the inversion formula of Muskhelishvili [41, 48] for unbounded dislocation density at the crack tip and the slip band tip.

$$D(x) = \frac{\beta\tau}{\pi A}\frac{x}{\sqrt{c^2 - x^2}} + \frac{k_1}{\pi^2 A} f(x; c, a) \tag{26}$$

$$\beta = 1 - \frac{2k_1}{\pi\tau}\arccos\left(\frac{a}{c}\right) \tag{27}$$

The microscopic stress intensity factor K^m at the tip of the slip band is similar to the crack tip stress intensity factor and is defined as

$$K^m = \pi A\sqrt{2\pi}\lim_{x\to c}\left[\sqrt{c - x}D(x)\right] \tag{28}$$

$$= \beta\tau\sqrt{\pi c} \tag{29}$$

The CTSD is

$$\phi^t = \frac{\beta\tau}{\pi A}\sqrt{c^2 - x^2} + \frac{2k_1 a}{\pi^2 A}\ln\frac{c}{a} \tag{30}$$

As the crack grows, K^m increases. For the crack to overcome the grain boundary obstacle and propagate into the subsequent grain, K^m must exceed the critical microscopic stress intensity factor K^m_{crit} provided by the grain boundary. If as $a \to c$,

K^m does not exceed K^m_{crit}, then the CTSD $\rightarrow$ 0 and the crack growth arrest. If K^m exceeds K^m_{crit}, the slip band tip propagates into the next grain and a condition called the *propagating slip band* exist.

The solution for the propagated slip band was obtained by Tanaka *et al.* [77]. The equilibrium condition is the same as Eq. 17 except

$$\tau^0 = \begin{cases} \tau & x < a \\ \tau - k_1 & a < x < L \\ \tau - k_2 & L < x < c \end{cases}$$

where k_2 is the frictional stress in the second grain. The size of the slip band zone is determined from the condition of vanishing dislocation density at the slip band tip.

$$\arccos\frac{a}{c} + \left(\frac{k_2}{k_1} - 1\right)\arccos\frac{L}{c} = \frac{\pi\tau}{2k_1} \tag{31}$$

The dislocation density and CTSD are determined in a similar manner as before.

$$D(x) = \frac{k_1}{\pi^2 A} f(x;c,a) + \frac{(k_2 - k_1)}{\pi^2 A} f(x;c,L) \tag{32}$$

$$\phi^t = \frac{2k_1 a}{\pi^2 A}\ln\frac{c}{a} + \frac{(k_2 - k_1)}{\pi^2 A} g(a;c,L) \tag{33}$$

$$g(a;c,L) = L\ln\left|\frac{\sqrt{c^2 - L^2} + \sqrt{c^2 - a^2}}{\sqrt{c^2 - L^2} - \sqrt{c^2 - a^2}}\right| - a\ln\left|\frac{a\sqrt{c^2 - L^2} + L\sqrt{c^2 - a^2}}{a\sqrt{c^2 - L^2} - L\sqrt{c^2 - a^2}}\right| \tag{34}$$

Tanaka *et al.* [84] solve for the case in which the slip band extends over several grains as shown in Fig. 5. If the crack tip is in the j^{th} grain and the slip band is in the n^{th} grain, the equilibrium condition is the same as Eq. 17 except

$$\tau^0 = \begin{cases} \tau & x < a \\ \tau - k_j & a < x < L_j \\ \vdots & \vdots \\ \tau - k_n & L_{n-1} < x < c \end{cases}$$

The size of the slip band zone can be found from

$$\frac{\pi\tau}{2} - k_j \arccos\frac{a}{c} - \sum_{i=j+1}^{n} (k_i - k_{i-1}) \arccos\left(\frac{L_{i-1}}{c}\right) = 0 \tag{35}$$

The CTSD is given by

$$\phi^t = \frac{2k_j a}{\pi^2 A} \ln\frac{c}{a} + \sum_{i=j+1}^{n} \frac{(k_i - k_{i-1})}{\pi^2 A} g(a; c, L_{i-1}) \tag{36}$$

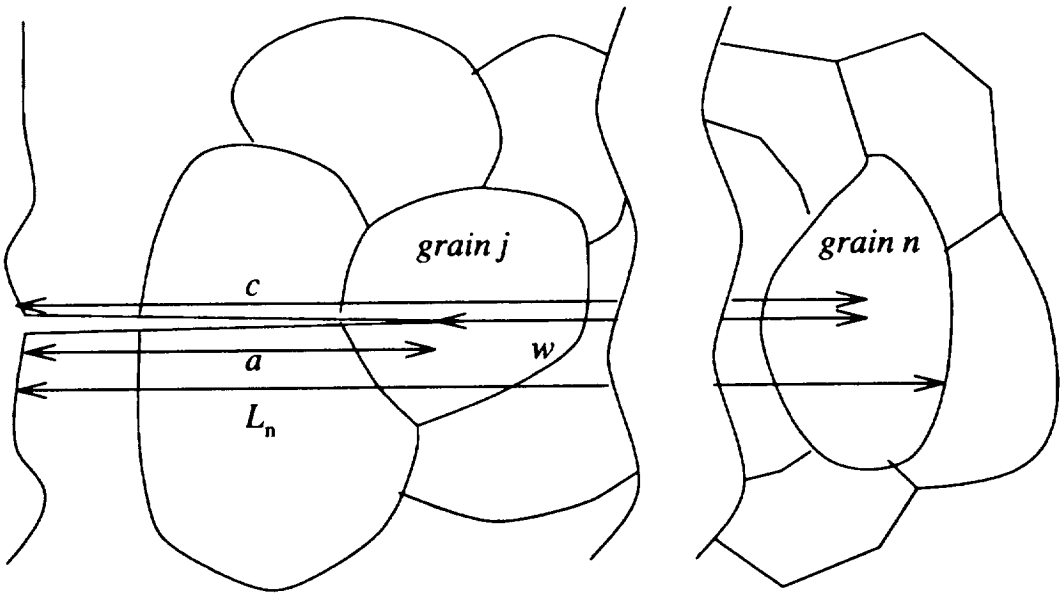

Figure 5: Crack tip slip band in multiple grains.

For the crack tip in the j^{th} grain and the slip band blocked in the n^{th} grain, the size of the slip band zone is

$$\omega = L_n - a \tag{37}$$

The CTSD is given by

$$\phi^t = \frac{\beta\tau}{\pi A}\sqrt{c^2 - a^2} + \frac{2k_j a}{\pi^2 A} \ln\frac{c}{a} + \sum_{i=j+1}^{n} \frac{(k_i - k_{i-1})}{\pi^2 A} g(a; c, L_{i-1}) \tag{38}$$

$$\beta = 1 - \frac{2k_j}{\pi\tau}\arccos\left(\frac{a}{c}\right) - \sum_{i=j+1}^{n}\frac{2(k_i - k_{i-1})}{\pi\tau}\arccos\left(\frac{L_{i-1}}{c}\right) \tag{39}$$

The microscopic stress intensity factor is

$$K_m = \beta\tau\sqrt{\pi c} \tag{40}$$

The above model allows for grain to grain variation in grain size and frictional stress.

In the present study, the Tanaka *et al.* [77] model is extended to include the variation in the microstress and the grain orientation by allowing grain to grain variation in the applied resolved shear stress τ.

Consider a crack with the crack tip in the j^{th} grain and the slip band tip in the n^{th} grain. The equilibrium condition is the same as Eq. 17 except

$$\tau^0 = \begin{cases} \tau_j & x < a \\ \tau_j - k_j & a < x < L_j \\ \vdots & \vdots \\ \tau_n - k_n & L_{n-1} < x < c \end{cases}$$

For the propagated slip band, the size of the slip band zone can be found from

$$\frac{\pi\tau_j}{2} - k_j\arccos\frac{a}{c} - \sum_{i=j+1}^{n}((\tau_{i-1} - k_{i-1}) - (\tau_i - k_i))\arccos\left(\frac{L_{i-1}}{c}\right) = 0 \tag{41}$$

The CTSD is given by

$$\phi^t = \frac{2k_j a}{\pi^2 A}\ln\frac{c}{a} + \sum_{i=j+1}^{n}\frac{(\tau_{i-1} - k_{i-1}) - (\tau_i - k_i)}{\pi^2 A}g(a; c, L_{i-1}) \tag{42}$$

For the blocked slip band, the size of the slip band zone is

$$\omega = L_n - a \tag{43}$$

The CTSD is given by

$$\phi^t = \frac{\beta\tau}{\pi A}\sqrt{c^2-a^2} + \frac{2k_j a}{\pi^2 A}\ln\frac{c}{a} + \sum_{i=j+1}^{n}\frac{(\tau_{i-1}-k_{i-1})-(\tau_i-k_i)}{\pi^2 A}g(a;c,L_{i-1}) \quad (44)$$

$$\beta = 1 - \frac{2k_j}{\pi\tau_j}\arccos\left(\frac{a}{c}\right) - \sum_{i=j+1}^{n}\frac{2((\tau_{i-1}-k_{i-1})-(\tau_i-k_i))}{\pi\tau_j}\arccos\left(\frac{L_{i-1}}{c}\right) \quad (45)$$

The microscopic stress intensity factor is

$$K_m = \beta\tau\sqrt{\pi c} \quad (46)$$

The solution for mode I loading is easily obtained through the following substitutions:

$$\tau \rightarrow \sigma$$

$$\text{CTSD} \rightarrow \text{CTOD}$$

Modeling the Physical Microstructure

Simplified characterizations of the physical geometry of the material microstructure have been assumed for small crack growth models presented in the literature. Most all of the probabilistic models consider only surface crack growth through a linear array of grains in which the grain size is the only random variable [83, 85, 86, 87]. Bataille and Magnin [16] assume uniform grain size but vary the orientation of the grains. They also consider a grain boundary blockage factor that is uniform throughout. Tanaka *et al.* [84] consider a linear array of grains with variation in grain size, frictional stress, and critical microscopic stress intensity factor.

Sun *et al.* [88] and Tanaka *et al.* [84] adopted the concept of microstructural dissimilitude [70] to model crack growth into the material volume. Both researchers assume that as the crack grows into the volume, the crack interrogates a 2-dimensional

array of space filling uniform hexagonal grains as shown in Fig. 6. As the crack grows, the crack front is either in position 1, 2, 3, or 4, etc. and the crack front interrogates n grains where $n = 1, 4, 7, 10$, etc. Sun *et al.* considers only variations in the orientation and describes the effective orientation M_{eff} as the simple arithmetic average orientation of the grains in which the crack front lies.

$$M_{eff} = \frac{\sum_{j=1}^{n} M_j}{n} \tag{47}$$

Tanaka *et al.* also defines the effective properties using a simple arithmetic averaging technique. They consider the variation in grain size and frictional stress. Although the above models are simple, the concepts of microstructural dissimilitude and effective material properties are important because they allows the two dimensions material variations to be approximated with a quasi one dimensional representation.

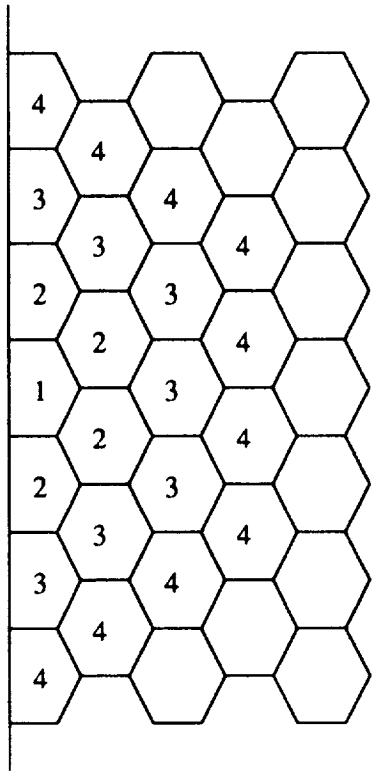

Figure 6: Array of hexagonal grains.

The concept of microstructural dissimilitude is applied in the current research, however, the effective material properties are not based on uniform hexagonal grains.

Consider a random array of grains as shown in Fig. 7. A crack nucleates in the surface grain X_0 and then grows as a semi-circle through zones in which the effective material properties are uniform. The boundaries of the zones are represented by the concentric half circles. The zones are composed of grains represented by the semi-circular segments. The arc length of the semi-circular segments is a random variable equal to the grain diameter. The surface grains are represented by the intersection of the zones and the surface. This representation differs from the array of space filling uniform hexagonal grains in that the number of grains in each zone is random.

After successful crack nucleation, the crack grows from grain X_0 into zone 1. In the example shown in Fig. 7, zone 1 contains three grains. The surface length l_1 of zone 1 is the simple arithmetic average of the grain diameters.

$$l_1 = \frac{d_{11} + d_{12} + d_{13}}{3} \tag{48}$$

The effective material property $P_{1_{eff}}$ of zone 1 is the average of the properties of the individual grains P_{1i} weighted with the area of the grain. (In the current study P_{eff} represents the local frictional strength k or the local applied stress τ.)

$$P_{1_{eff}} = \frac{P_{11}d_{11}^2 + P_{12}d_{12}^2 + P_{13}d_{13}^2}{d_{11}^2 + d_{12}^2 + d_{13}^2} \tag{49}$$

In the n^{th} zone composed of j grains, the surface length is

$$l_n = \frac{\sum_{i=1}^{j} d_{ni}}{j} \tag{50}$$

and the effective material property is

$$P_{n_{eff}} = \frac{\sum_{i=1}^{j} P_{ni}d_{ni}^2}{\sum_{i=1}^{j} d_{ni}^2} \tag{51}$$

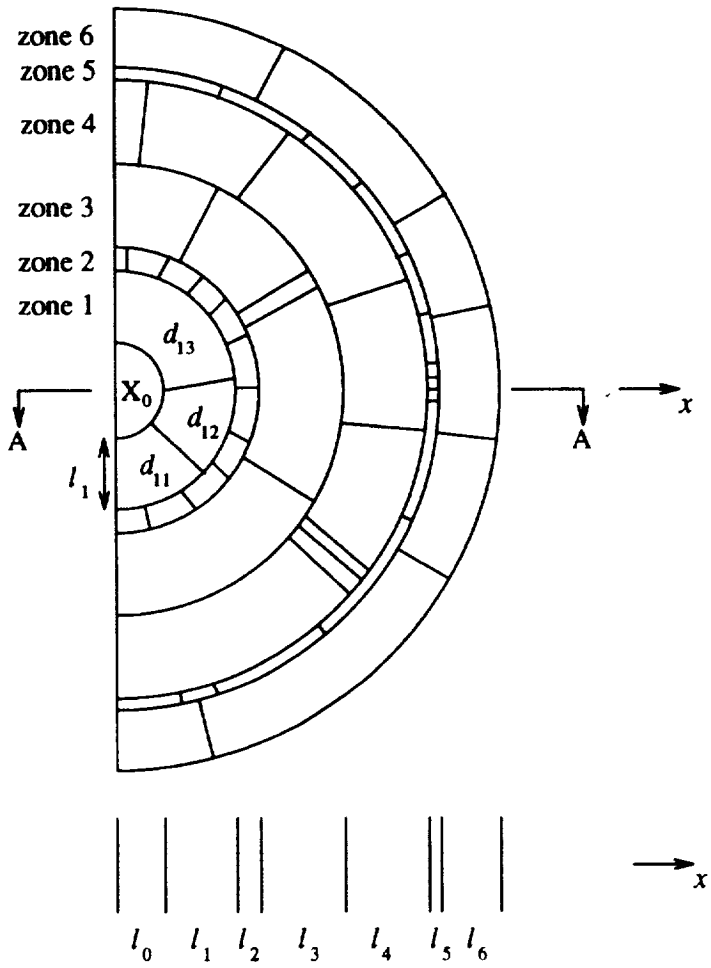

Figure 7: Array of random grains.

As the crack becomes long, l approaches the mean grain size and P_{eff} approaches the bulk properties.

Using the concepts of effective material properties, crack growth is modeled as 1-dimensional. Consider a cut along the x-axis (Section A-A in Fig. 7). The fatigue damage is modeled as a 1 dimensional crack growing through zones of varying size l_n and varying effective material properties $P_{n_{eff}}$.

The above microstructural modeling technique is approximate and does not capture some of the nuances of crack-microstructure interactions. In particular, the

model does not allow for spatial variation of properties along the crack front which can cause a non-smooth or ragged crack front shape. If the crack front encounters strong grains (due to unfavorable orientation or high frictional stress) in a matrix of weaker grains, the crack front will retard in the region near the strong grains and tunnel in the region of the weak grains. However, crack growth mechanisms tends to have a smoothing effect on the crack front shape. The crack front will tunnel around the blockage until the shape of the crack front at the blockage is such that the stress intensity overcomes the blockage and the crack front resumes its smooth shape [31]. If the blockage is not overcome, the crack front will not continue to tunnel. The crack growth will arrest.

CHAPTER V

LONG CRACK GROWTH

The linear elastic crack growth is modeled using the Paris law representation of a surface crack in a semi infinite body subjected to a constant stress cycle.

$$\begin{aligned} \frac{da}{dN} &= C\Delta K^n \\ \Delta K &= \beta \Delta s_{xx} \sqrt{a} \end{aligned}$$

where a is the crack length, N is cycles, ΔK is the stress intensity factor, Δs_{xx} is the stress range, β is the geometry constant $(1.12\sqrt{\pi})$, and C and n are material properties.

Expanding ΔK and integrating both sides

$$C(\beta \Delta s_{xx})^n \int_0^{N_g} dN = \int_{a_i}^{a_f} a^{-\frac{n}{2}} da$$

$$N_g = \frac{a_i^{1-\frac{n}{2}} - a_f^{1-\frac{n}{2}}}{C\Delta s_{xx}^n \beta^n (\frac{n}{2} - 1)}, n \neq 2 \tag{52}$$

where, N_g is the number of cycles needed for the crack to grow to failure, a_i is the initial crack size, and a_f is the failure crack size.

If $n > 2$ and $a_i \ll a_f$, then $a_i^{1-\frac{n}{2}} \gg a_f^{1-\frac{n}{2}}$ and Eq. 52 can be written as

$$N_g = \frac{a_i^{1-\frac{n}{2}}}{C\Delta s_{xx}^n \beta^n (\frac{n}{2} - 1)} \tag{53}$$

CHAPTER VI

RANDOM VARIABLES

Recent developments in the literature allow for the investigation of the statistical characteristics of several of the variables used in the crack nucleation and small crack growth models.

Grain Size

Empirical observations have indicated that the scatter in grain size for "natural grain growth" i.e., cast polycrystalline structures, is insensitive to material. This has been observed in pure metals, complex alloys, and inorganic ceramics [89]. This phenomenon has been attributed to the well behaved kinetics that determine natural grain growth.

Kurtz and Carpy [90] performed extensive grain volume measurements on Ni-Zn ferrites by way of planar sectioning, and describe the grain size by the equivalent spherical volume diameter. They determined the grain size distribution for 7 different mean grain size microstructures measuring several thousand grains for each microstructure. They found the COV to vary between 0.3 and 0.4. The COV was independent of mean grain size. The distribution was accurately described by a lognormal distribution with the maximum to mean grain size ratio of about 2.7.

Kumar *et al.* [91] investigated the grain size distribution using Monte Carlo techniques and a Voronoi tessellation technique which closely model the grain topography of polycrystals. They found a COV of about 0.4. The lognormal distribution was a

good fit up to about 5000 grains. Simulating greater than 100,000 grains, they found the gamma distribution to be a best fit.

The gamma distribution may well be an artifact of the modeling technique and not intrinsic to the grain size distribution. Voronoi tessellation uses the Poisson process to generate the grain geometry and the gamma distribution is directly related to the Poisson process [92]. In the present study, a lognormal distribution with a COV of 0.4 as shown in Fig. 8 will be assumed.

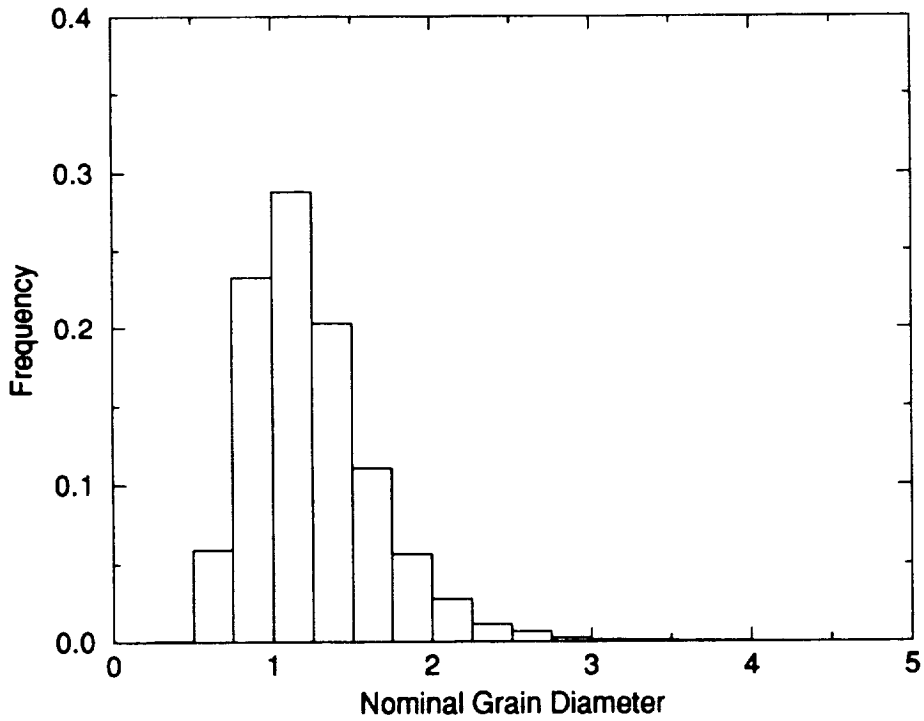

Figure 8: Grain diameter distribution.

The bulk of the grains measured in the above research were interior grains. A distinction must be made between the size of the surface grains and those in the interior. Although the surface grains may account for only a small fraction of the total grains within a component, understanding the properties of the surface grains is paramount because they play an important role in crack nucleation and small crack

growth.

The surface effectively slices each grain in a random manner such that

$$d_s = d\cos\theta \tag{54}$$

where d_s is the surface length, d is the grain diameter, and θ is the random angle of incidence as shown in Fig. 9. For an arbitrary cut through the grain, θ is uniformly distributed between 0 and $\pi/2$. The distribution of d_s can be determined from

$$d_s = d\cos\left(\frac{\pi}{2}u\right) \tag{55}$$

where d is lognormally distributed as shown in Fig. 8 and u is the standard uniform random variable.

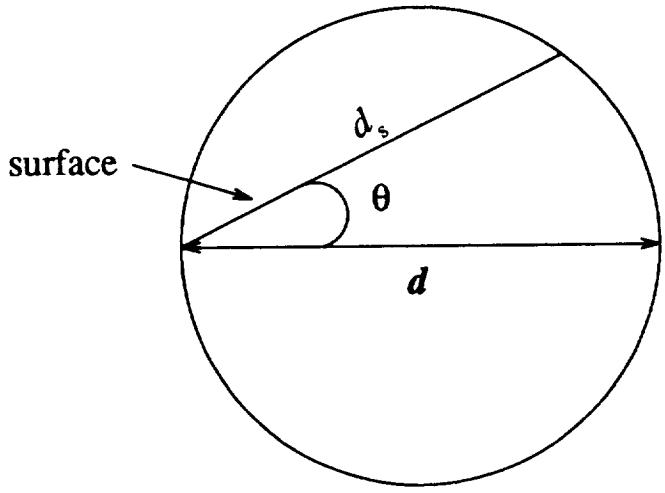

Figure 9: Surface slicing a grain.

Monte Carlo simulation was used to evaluate the distribution of d_s as shown in Fig. 10. Comparing Fig. 10 to Fig. 8 shows that the average diameter of the surface grains is smaller than the interior grains. The increase width of the surface grain

distribution indicates that the scatter in the surface grains diameter is larger than the interior grains.

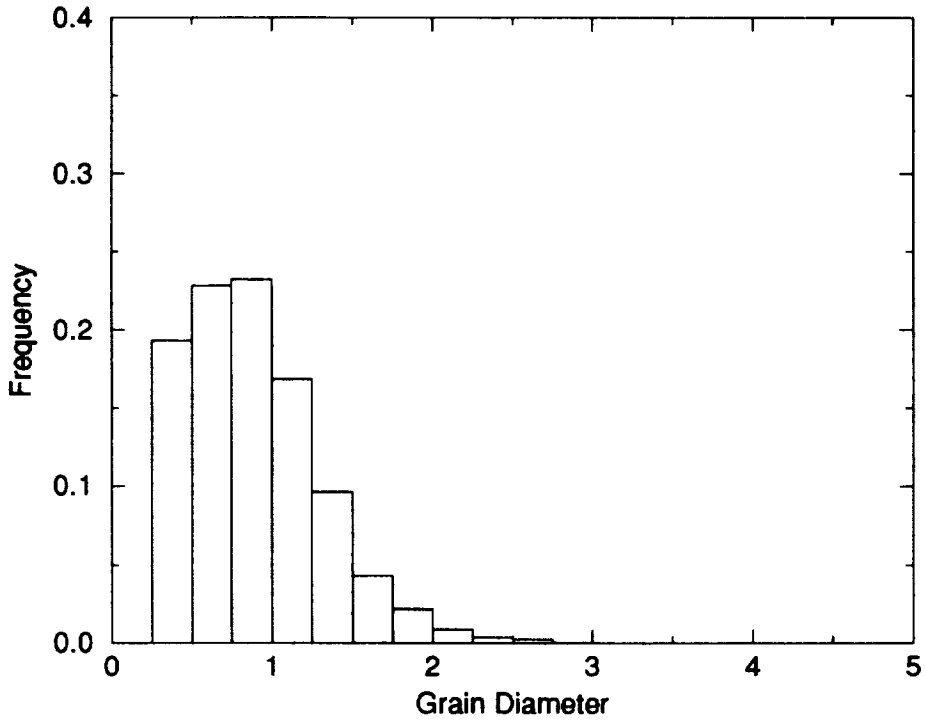

Figure 10: Surface grain size distribution.

Applied Micro-Stress

Because each grain acts as an anisotropic single crystal, the actual loading on an individual grain is caused by the deformation of the surrounding grains, which are in turn loaded by the deformations of each of their surrounding grains. Therefore, the micro-stress distribution is a function of the anisotropic deformation of all on the grains that compose the structure.

Barenblatt [93] proposed a theoretical model to describe the micro-stress field. Many simplifying assumptions were necessary to make the model tractable.

Kozaczek *et al.* [94] investigated the micro-stress field for a single phase nickel

alloy using finite elements and Voronoi tessellation to produce a model that closely approximates the microstructure. They modeled a structure with 500 grains. Each grain was modeled as an anisotropic single crystal with 40 to 50 finite elements per grain. An elastic analysis was performed in which a uniaxial macroscopic load was applied. The von Mises stress at the grain interiors could be described by a normal distribution with a mean equal to the applied macroscopic stress and a COV of 0.25. The stress distribution of the surface grains was found to be the same as the interior grains. The COV was a function of the elastic anisotropy of the material.

In this paper the micro-stress will be assumed to have a normal distribution with a mean value equal to the applied load s_{xx} and a COV of 0.25.

Grain Orientation

Since plastic flow occurs on slip planes in particular directions, τ is a function of grain orientation and the applied stress. Consider a single grain with slip on a single plane in the grain as shown in Fig. 11. The resolved shear stress is

$$\tau = m s_{xx}$$

$$m = \cos\zeta \cos\lambda$$

where s_{xx} is the applied uniaxial stress, ζ is the angle from the slip plane normal to the loading axis, and λ is the angle from the slip direction to the loading axis. m is referred to as the Schmid factor [95]. τ is a maximum at $\zeta = \lambda = 45°$, $m = \frac{1}{2}$. τ is zero when the tensile axis is perpendicular to the slip plane ($\lambda = 90°$) or parallel to the slip plane ($\zeta = 90°$).

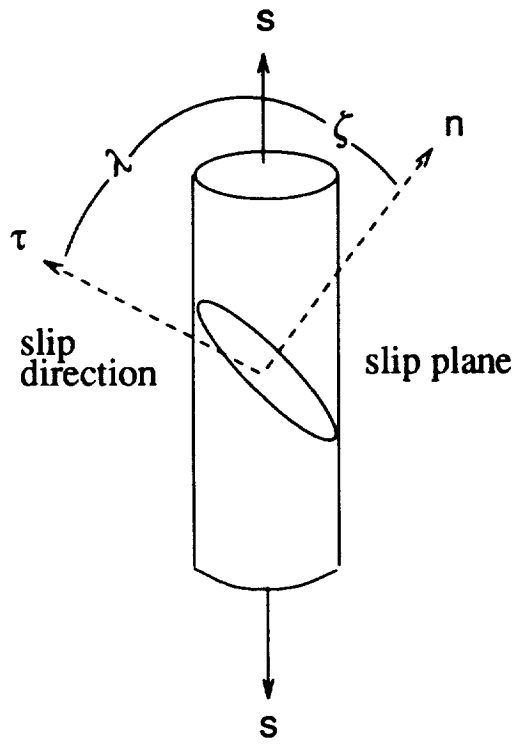

Figure 11: Single grain with axial load s.

In metallic structures, slip can occur on many planes in several directions. Face-centered cubic alloys prefer $\{111\}\langle 110\rangle$ slip. Body-centered cubic structures exhibit $\{110\}\langle 111\rangle$, $\{112\}\langle 111\rangle$, and $\{123\}\langle 111\rangle$ operative slip. However, in the case of fatigue at low stresses, cracking has been shown to prefer the $\{110\}\langle 111\rangle$ slip system for some low carbon steels [40, 96].

Twelve potential slip systems are available for $\{111\}\langle 110\rangle$ or $\{110\}\langle 111\rangle$ slip. The orientation of the grain does not have to change much before the resolved shear stress becomes high on another slip system. All orientations for cubic structures can be defined within the standard stereographic triangle [97].

The orientation dependence of the reciprocal Schmid factor

$$m = \frac{1}{M} = \frac{1}{\cos\phi\cos\lambda}$$

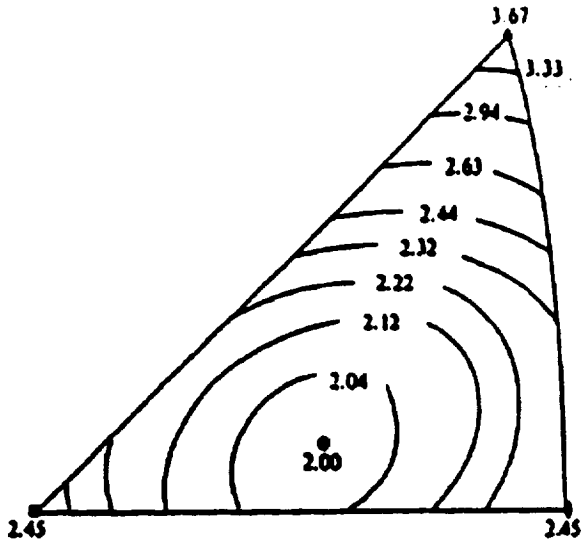

Figure 12: Orientation dependence of the reciprocal Schmid factor M (from Barrett).

is shown in Fig. 12 [98] and the resolved shear stress can be expressed as

$$\Delta\tau = \frac{\Delta s_{xx}}{M}$$

Figure 12 represents axially loaded grains that are free to deform such that slip occurs on a single plane. However, grains within a polycrystalline aggregate are not free to deform but are constrained by neighboring grains.

Taylor [99] determined the equivalent to the reciprocal Schmid factor, M, for axisymmetric flow in a face-centered cubic polycrystal. He assumed the frictional stress was the same for each slip system. He also assumed that each grain is acted upon by the same applied strain as the macroscopic strain.

$$\begin{aligned} \epsilon_{yy} &= \epsilon_{zz} = -\frac{1}{2}\epsilon_{xx} \\ \epsilon_{yz} &= \epsilon_{zx} = \epsilon_{xy} = 0 \end{aligned}$$

where x, y, z refer to the global axis. For general constrained deformation, slip from five independent slip systems is needed to accommodate the five independent strains

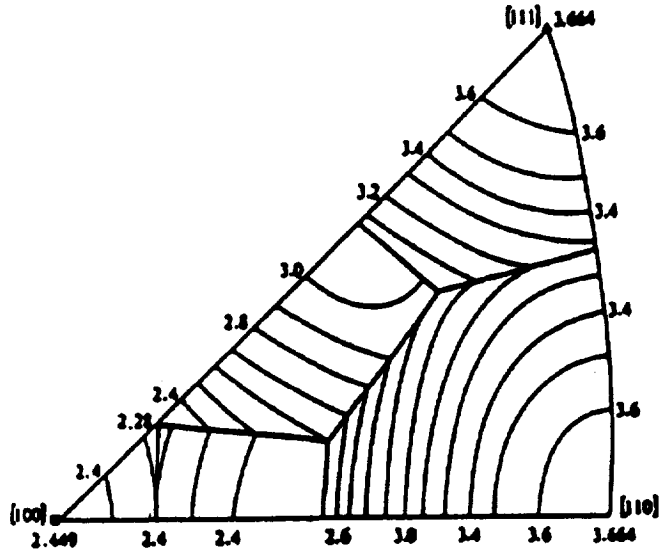

Figure 13: Orientation dependence of the Taylor factor M (from Hasoford and Backofen).

$\epsilon_{11}, \epsilon_{22}, \epsilon_{12}, \epsilon_{23}, \epsilon_{31}$, where $1, 2, 3$ refer to the grain axis. (ϵ_{33} is not independent because $\epsilon_{11} + \epsilon_{22} + \epsilon_{33} = 0$ for constant volume.) Taylor assumed the five active slip systems are those for which the sum of the shear strains is a minimum. Bishop and Hill [100] later showed that the Taylor analysis is equivalent to a maximum work principle. M for the Taylor analysis is shown in Fig. 13 [101]. This quantity is referred to as the Taylor factor. Chin and Mammel [102] developed a computer model based on the Taylor analysis and found the Taylor factor for slip on other orientations in cubic polycrystals.

Crack nucleation takes place on the surface grains. It is difficult to determine M for the surface grains which are not as constrained as grains embedded in the interior. Surface grains are able to accommodate more strain on the primary slip system. Although slip band formation and crack nucleation on secondary planes is not uncommon, experimental evidence shows that cracks tend to nucleate on the primary slip plane [49]. In reality, the deformation of surface grains is somewhere

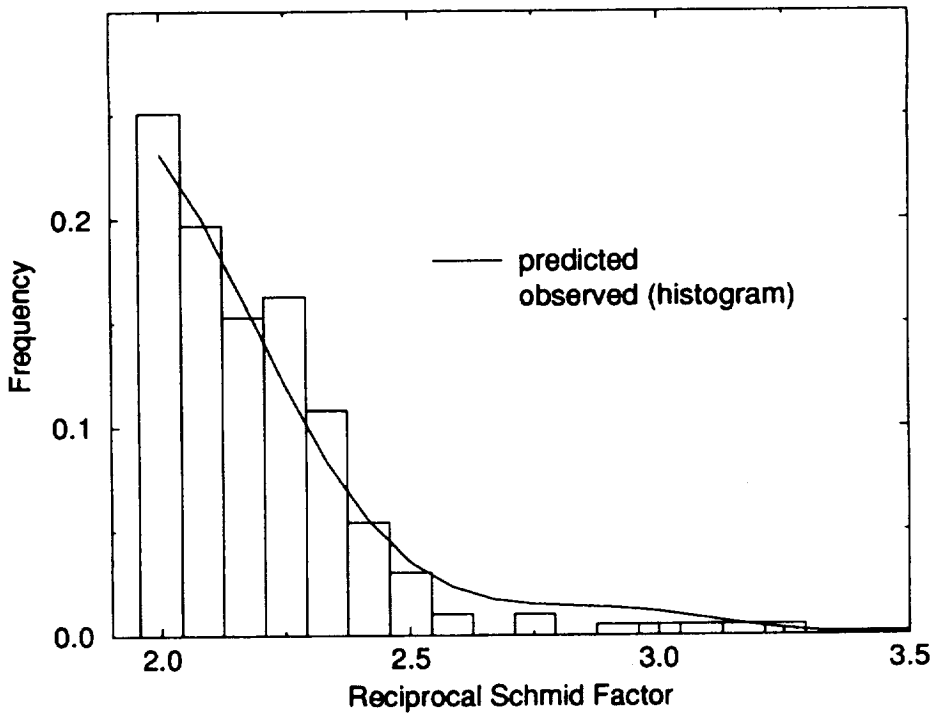

Figure 14: Probability mass function of the reciprocal Schmid factor.

between free deformation and fully constrained.

The orientations of the grains of an untextured polycrystalline material can be expressed as a uniform distribution of points within the stereographic triangle. Using M as defined by the reciprocal Schmid factor in Fig. 12, the probability distribution function (PDF) and the cumulative distribution function (CDF) of M are shown in Figs. 14 and 15 respectively. The mean value of the distribution is 2.21 which is in agreement with other analytical findings [98]. The predicted PDF of M compares favorably to the experimentally determined reciprocal Schmid factor (Fig. 14) for 203 surface grains of an untextured pure iron [96]. The CDF does not seem to fit any standard distribution and is therefore expressed by the fifth order polynomial with the coefficients shown in Fig. 15.

Using M as defined in Fig. 13, the PDF and the CDF of the Taylor factor for

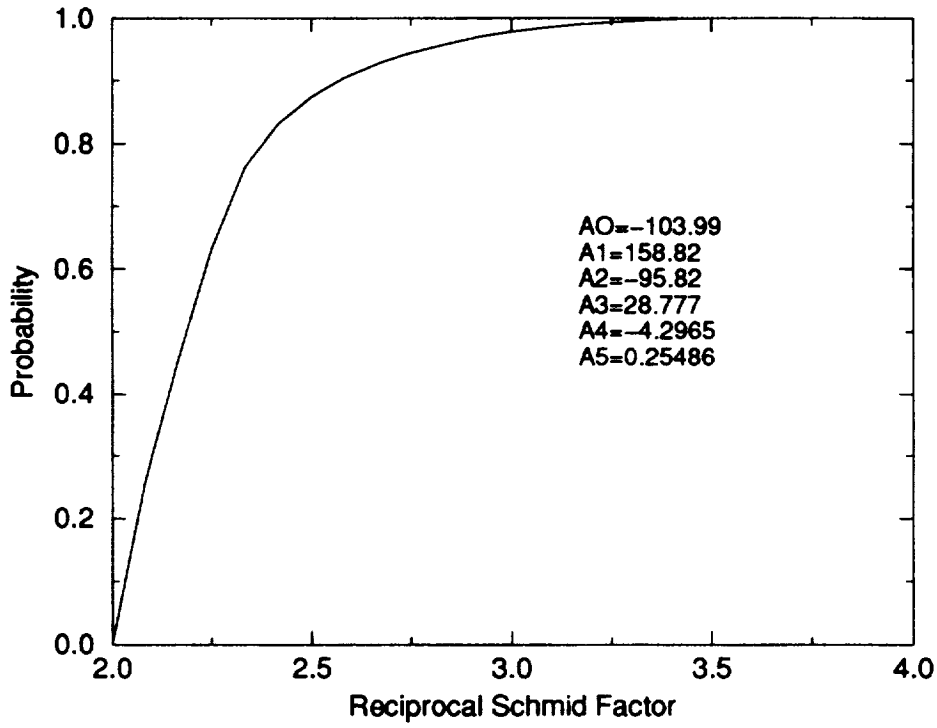

Figure 15: Cumulative distribution function of the reciprocal Schmid factor with the coefficients for a fifth order polynomial curve fit.

an untextured polycrystal are shown in Fig. 16 and 17 respectively. The mean value of the distribution is 3.07 which is in agreement with analytical and experimental findings [98]. The predicted PDF of M determined in the present study compares favorably to the analytical results of Sun *et al.* [88]. They determined the PDF of the Taylor factor using the computer solution of Chin and Mammel [102] and considering all possible crystallographic orientations. The distribution is close to uniform but the CDF is more accurately expressed by the fifth order polynomial with the coefficients shown in Fig. 17.

The reciprocal Schmid factor will be used to describe the surface grains and the Taylor factor will be used to describe the interior grains in the present study.

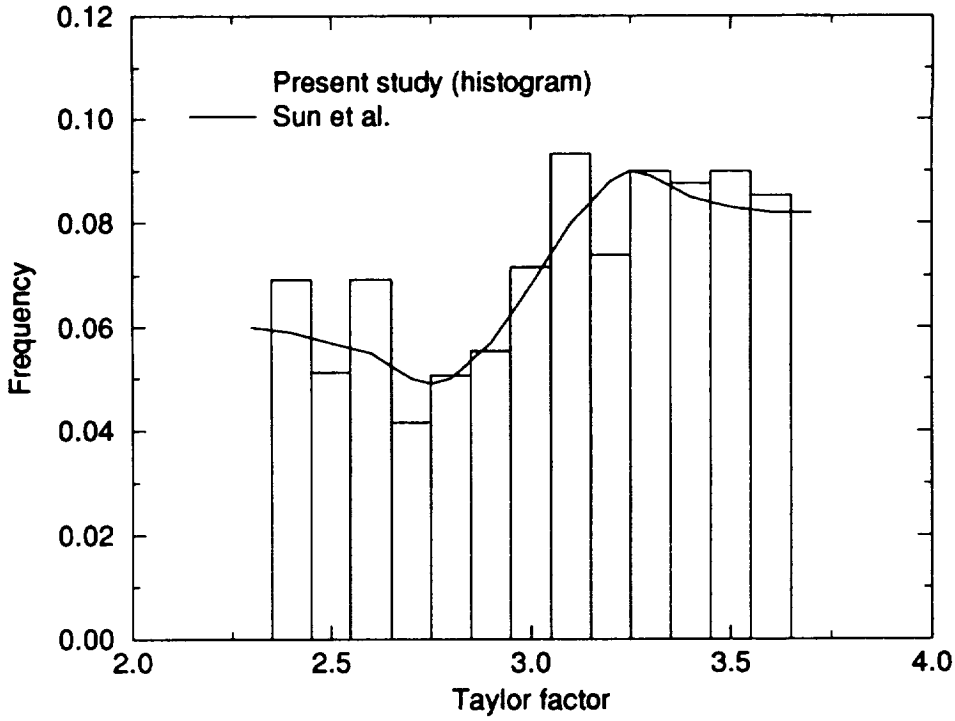

Figure 16: Probability mass function of the Taylor factor.

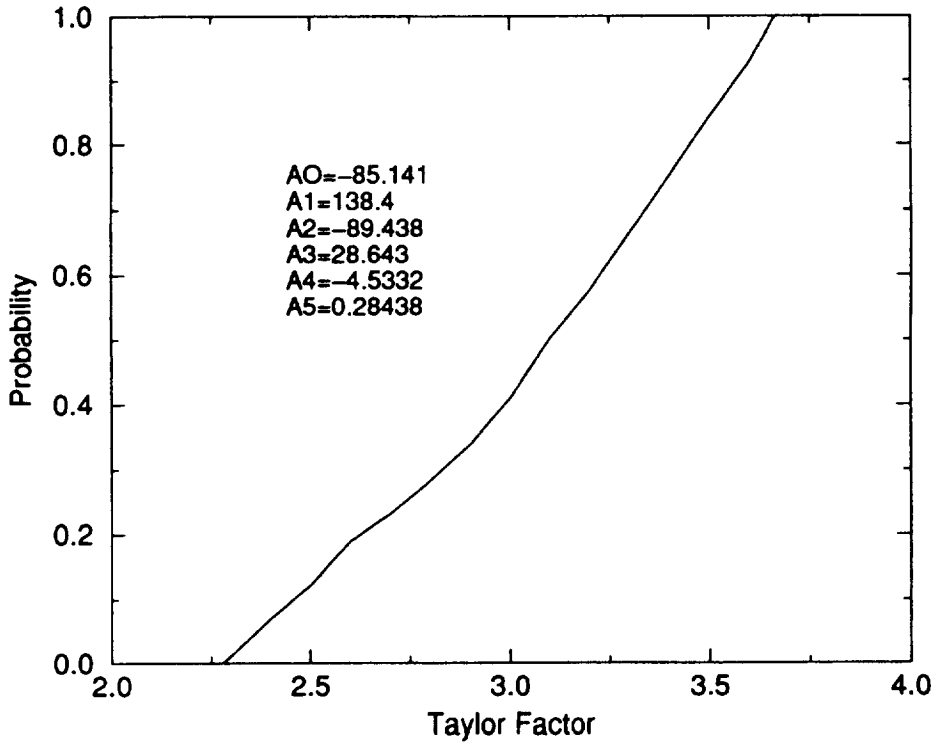

Figure 17: Cumulative distribution function of the Taylor factor with the coefficients for a fifth order polynomial curve fit.

Frictional Shear Stress

The frictional stress is the stress which must be overcome for dislocations to move within a grain. The frictional stress can be thought of as the local yield stress. Because of the crystallographic orientation of the grain, yielding takes place on well defined planes (in the low Γ planar slip alloys). Experimental observations have shown that the frictional stress is nearly uniform across the grain [55].

There is little direct data available in the literature on the statistical distribution of the frictional stress. A rigorous numerical determination of the grain–to–grain scatter in frictional stress has not been made. However, empirical observations provide some insight into the behavior of the scatter.

Taira *et al.* [10] experimentally observed the minimum cyclic stress for which slip bands formed in three different mean grain size microstructures of low-carbon steel. The applied stress was below the fatigue limit and slip bands formed in very few grains. They found that the the minimum frictional stress is independent of mean grain size. The minimum frictional stress was nearly equal to the frictional stress predicted by the Petch relationship for the fatigue limit, expressed as

$$\sigma_{fl} = k_{fl} + \frac{K'^{m}}{\sqrt{d}} \tag{56}$$

where σ_{fl} is the fatigue limit, k_{fl} is the frictional stress of the grains participating in fatigue, and K'^{m} is the microscopic stress intensity factor.

Taira *et al.* used the Petch relationship for flow stress to determine the frictional stress for applied loads up to 5% plastic strain. As the load increased more and more grains produced slip bands. An indication of the scatter can be made by comparing the frictional stress determined at high applied load to the frictional stress at low

applied load. At high applied load, many grains produce slip bands and this frictional stress may be thought of as the frictional stress of the average grain. At low applied load, only a few grains produce slip bands and this frictional stress may be thought of as the frictional stress of the weakest grain.

This method is not rigorous because the variation in the microstress is not taken into account. Also, it is difficult to determine the shape of the distribution. In the present study a two parameter Weibull distribution is assumed and fitted to the data in Taira *et al.* The parameters of the Weibull distribution are determined by taking the frictional stress determined from the 5% plastic strain test ($k_{.05} = 340MPa$) to be the frictional stress of the 50 percentile grain and the frictional stress from the fatigue limit test ($k_{fl} = 110MPa$) is taken to be the frictional stress of the 1 percentile grain. This gives a normalized Weibull distribution with a shape factor $\beta^w = 3.7$ and a characteristic value $\eta^w = 1.12$ which yields a mean value of 1 and a COV of 0.3. Tanaka *et al.* [84] indicate that a two parameter Weibull distribution with COV between 0.3 and 0.7 can be used to describe the frictional stress.

Critical Microscopic Stress Intensity Factor

The critical microscopic stress intensity factor is a measure of the blockage provided by the grain boundary. The small crack must be able to produce a stress intensity factor at the slip band tip greater than the critical microscopic stress intensity factor if slip is to propagate into the next grain. The blockage is attributed to the difference in orientation between the grains and the inherent strength of the grain boundary itself.

de los Rios and his co-workers [103, 104] have developed a short crack model in

which the variation in small crack growth is attributed to the variation in grain orientations. They develop a microscopic stress intensity factor that is proportional to the difference in the Taylor factor between the grains [88]. Thus, there is no grain boundary blockage effect between two grains with the same Taylor factor. This approach is questionable. Figure 13 shows that grains with vastly different orientations can have the same Taylor factor ie., there is not a one to one mapping between Taylor factor and orientation.

The Petch relationship can be used to investigate the scatter in the microscopic stress intensity factor. Many investigations have shown that the slope in the Petch equation (K^m in Eq. 56) is constant as the load varies [10, 105, 106]. If it is assumed that at low applied stress, slip bands propagate across very few grain boundaries and at high stress, propagation takes place across many grain boundaries, the lack af variation in the Petch slope indicates a lack in variation in the grain blockage effect.

In the present study, the microscopic stress intensity factor is assumed to be deterministic.

Specific Fracture Energy

Chudnovsky and his co-workers [107, 108, 109] have investigated the spatial variation in specific fracture energy for brittle materials. They show that the specific fracture energy can be characterized by a three parameter Weibull distribution. However, their results are not directly applicable to metal alloys because the specific fracture energy in brittle materials is dominated by the surface energy, whereas the specific fracture energy in ductile materials is dominated by plastic work. There is no direct data available for the distribution of the plastic work for metallic alloys.

In this study, the specific fracture energy is assumed to be deterministic and equal to the plastic work.

Summary of Random Variables

Table 3 below summarizes the random variable distributions used in the present study.

Variable	Distribution Type	Distribution Parameters		Mean	COV
d	Lognormal	$\lambda = -0.076$	$\zeta = 0.39$	1	0.40
σ	Normal	mean = 1	std. dev = 0.25	1	0.25
k	Weibull	$\eta = 1.12$	$\eta = 3.7$	1	0.30
C	Lognormal	$\lambda = -0.045$	$\zeta = 0.3$	1	0.30
M_s	Curve Fit (Fig. 15)			2.21	0.08
M_t	Curve Fit (Fig. 17)			3.07	0.13

Table 3: Distributions used in the Monte Carlo Simulation

CHAPTER VII

MONTE CARLO SIMULATION MODEL

The distributions used in the Monte Carlo simulation are shown in Table 3. The input variables are shown in Table 4. Normalized distributions are used for d, σ, k, and C. This allows the average values to be easily changed without having to re-evaluate the distribution parameters. The distribution parameters only need re-evaluated if a change in COV is desired. The orientation factors are not normalized. A change in the average value of the orientation factor would require texturing the microstructure. Figures 12 and 13 would no longer be valid and new representations in the stereographic triangle would be required.

Variable	Description
d_{avg}	Average Grain Diameter
τ_{avg}	Bulk Applied Stress
k_{avg}	Bulk Frictional Stress
C_{avg}	Average Paris Law Coefficient
n	Paris Law Exponent
β'	CTOD Law Coefficient
K^M_{crit}	Critical Microscopic Stress Intensity Factor
da	Crack Growth Law Interval
$Area$	Surface Area of Component
S_N	Number of Samples

Table 4: Input to the Monte Carlo Simulation

The basic flow of the Monte Carlo simulation is outlined as follows. A crack is nucleated in each surface grain of a component. Each crack goes through the small crack growth phase and long crack growth phase. The total life associated with each

crack is the summation of the cycles in the crack nucleation, small crack growth, and long crack growth phases. The life of the component is equal to the minimum total life of all of the cracks. In the rest of this section, the details of the simulation are described.

Crack Nucleation

A surface grain is simulated by generating d, σ, k, and M_s from the appropriate distributions. The size of the surface grain d^s is generated using Eq. 55. The number of cycles need to crack the surface grain is determined using Eq. 10. The microscopic stress intensity factor K^m is calculated using Eq. 28.

If $K^m < K^m_{crit}$ then the crack arrests at the grain boundary. The next surface grain is generated by repeating the process. If $K^m > K^m_{crit}$ then the crack will continue into the small crack phase.

Small Crack

In the small crack phase, the microstructure surrounding the crack nucleating grain is first simulated.

Region of microstructural dissimilitude

Consider a crack nucleating at X_0 in Fig. 18A. Zone 1, directly in front of the crack, is simulated first. The properties d, σ, k, and M_s of grain g^s_{11} are generated using the appropriate distributions. The grain is a surface grain, therefore, the size of the grain d^s_{11} is generated using Eq. 55 and the Schmid factor orientation is assumed.

The arc length l_{arc1} is determined by

$$l_{arc1} = \frac{\pi}{2}\left(\frac{L_0}{2} + \frac{d_{11}^s}{2}\right) = \frac{\pi}{4}(L_0 + d_{11}^s) \tag{57}$$

If $d_{11}^s > l_{arc1}$ then the grain fills the zone and d_{11}^s is set equal to l_{arc1}. The properties of zone 1 are those generated for g_{11}^s.

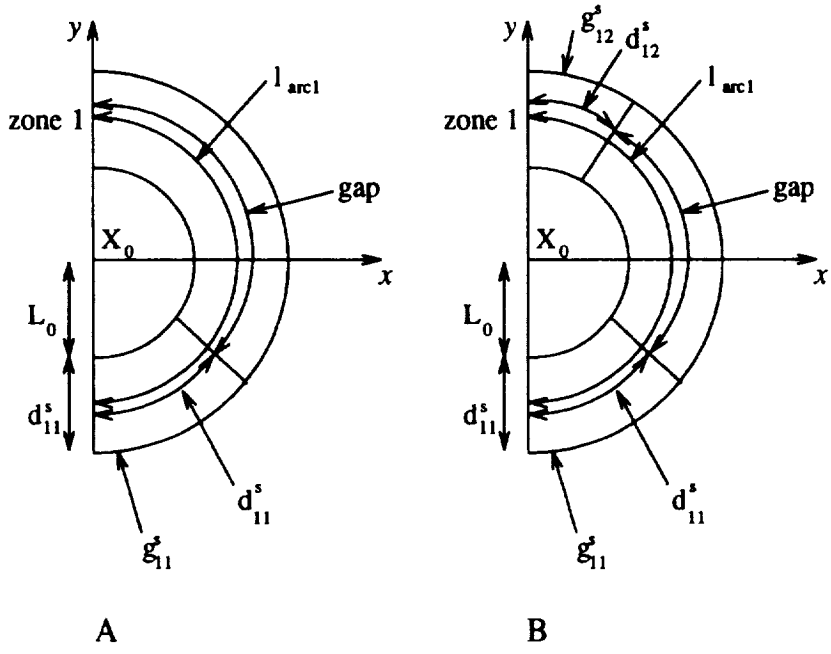

Figure 18: Geometry of microstructure

If $d_{11}^s < l_{arc1}$ then the grain does not fill the space. A gap remains of size

$$gap = l_{arc1} - d_{11}^s \tag{58}$$

The other surface grain g_{12}^s in zone 1 (see Fig. 18B) is generated with the appropriate properties. The size of the grain d_{12}^s is compared with the gap.

If $d_{12}^s > gap$ then the grain fills the gap and d_{12}^s is set equal to the gap. The effective properties of the zone 1 are calculated using Eqs. 50 and 51. If $d_{12}^s < gap$ then l_{arc1} is recalculated based on the average diameter of the 2 grains such that

$$l_{arc1} = \frac{\pi}{4}\left(L_0 + \frac{d_{11}^s + d_{12}^s}{2}\right) = \frac{\pi}{4}(L_0 + d_{1avg}^s) \tag{59}$$

A gap remains of size

$$gap = l_{arc1} - d_{11}^s - d_{12}^s \tag{60}$$

An interior grain is now generated with the appropriate properties. The Taylor analysis is used for the orientation factor. If the grain fills the gap, then the grain size is set equal to the gap and the effective zone properties are calculated using Eqs. 50 and 51. If the grain does not fill the gap, then the arc length and the gap are recalculated and grains are generated until the gap is filled. The effective properties of the subsequent zones are generated using the same technique.

Zones are generated until the effective material properties are within $\pm 10\%$ of the average material properties for three successive zones. Thus, the microstructure is generated until microstructural similitude is achieved. The number of zones and the total area of the zones is random and depends on the variation of the microstructural properties. Microstructures with small variations will have a smaller region of dissimilitude than microstructures with large variations.

Small crack growth

Once the crack has nucleated and penetrated the first grain boundary, the small crack growth stage begins. The equations governing small crack growth depend on the condition at the tip of the slip band as discussed in Chapter IV. First, the propagated

slip band phase is considered.

Propagated slip band

The crack tip is at L_0 in Fig. 18. The slip band tip is in zone 1.

If $\tau_{eff} > k_{eff}$ then the zone has yielded and the slip band tip has traversed to the next zone boundary. In this case, the propagated slip band phase requires zero cycles and the next phase of blocked slip band is considered.

If $\tau_{eff} < k_{eff}$ then the slip band has not yet reached the next zone boundary and the position of the slip band tip is determined using Eq. 41. An iterative technique is needed to solve Eq. 41 because it is not closed form. Newton's method is used with the convergence criteria that successive values be within $0.1da$, where da is the crack growth increment which is an input variable. (da must be some small fraction of the average grain diameter.) Once the location of the slip band tip has been determined, ϕ^t is evaluated using Eq. 42. The number of cycles needed for the crack tip to traverse a distance da is calculated by

$$dN = \frac{C'\phi^t}{da} \tag{61}$$

The new position of the crack tip is $a + da$. The process is repeated until the slip band tip reaches the next zone boundary. At this point, the blocked slip band phase begins.

Blocked slip band

The crack tip is located at a determined form the above propagated slip band routine. The slip band tip is blocked at the zone boundary. The microscopic stress intensity factor K^m is calculated using Eq. 46.

If $K^m > K^m_{crit}$ then the slip band tip successfully penetrates the zone boundary. In this case, the blocked slip band phase requires zero cycles and the propagated slip band phase is considered for the next zone.

If $K^m < K^m_{crit}$ then ϕ^t is calculated using Eq. 44. The number of cycles needed for the crack tip to traverse a distance da is calculated using Eq. 61. The new position of the crack tip is $a + da$. The process is repeated until the slip band tip penetrates the zone boundary or the crack growth arrests.

The slip band tip will penetrate the zone boundary when $K^m > K^m_{crit}$. With each successive iteration, the crack tip grows da and K^m increases. However, in Eq. 44, as a approaches L_j, ϕ^t approach 0. This causes dN to approach infinity in Eq. 61. Therefore, if $K^m < K^m_{crit}$ when $a = L_j$, the crack growth arrest. In other word, if the crack tip reaches the zone boundary and the stress intensity factor is still less than critical, the crack stops growing.

If the crack growth arrest, the next surface grain is generated. If the crack growth does not arrest, the slip band tip successfully penetrates the zone boundary and the propagated slip band phase is considered for the next zone.

The crack continues to grow through propagated and blocked phases of successive zones until the crack is arrest or the slip band tip has reached the end of the microstructural dissimilitude region at which point LEFM is assumed valid.

Long Crack Growth

Once the crack has reached the long crack growth stage there is no mechanism for blockage. The number of cycles spent in the long crack growth stage is calculated using Eq. 53 with C generated from the appropriate distribution.

Total life

The total number of cycles for the crack to grow to failure is the summation of cycles spent in each stage. The total number of cycles is stored. The next surface grain is generated and the entire process is repeated. Surface grains are generated until the area of all of the surface grains equal the surface area of the component. The specimen life is the minimum number of cycles to failure associated with the ensemble of surface grains.

It is not necessary to determine the total life of the crack initiated in each surface grain. If the total life of a crack is greater than the minimum life of the ensemble of previously generated surface grains, then the crack is not involved in in the component failure. Therefore, if the number of cycles exceeds the minimum previous life at any time during the simulation of a crack, the crack is rejected and the next surface grain is generated. This technique reduces, by many orders of magnitude, the number of cracks that need to be simulated to final failure.

Validating the computer program

The equations in the Monte Carlo simulation computer program were validated using MAPLE [110]. The equations were program in MAPLE and the numerical results were compared to those form the Monte Carlo simulation computer program.

The logic and flow of the Monte Carlo simulation computer program were partially validated through extensive use. Many different sets of input variables have been used and the reasonableness of the output has been examined. Internal variables and parameters such as distribution shapes and crack growth rates have been examined for reasonableness.

CHAPTER VIII

MODEL RESULTS

Crack Nucleation

The crack nucleation model of Eq. 10 has previously been investigated by Tryon and Cruse [111]. The study developed a first order reliability model to investigate scatter in fatigue crack nucleation. The results of the investigation are briefly presented here.

The predicted shape of the crack nucleation life distribution was similar to the experimentally observed shapes found in the literature. The COV of crack nucleation life was predicted to increase as the applied load decreased and the COV was independent of the mean grain size. These predictions are in agreement with the experimental findings.

Small Crack Growth

Small crack growth behavior is modeled using the small crack growth phase of the Monte Carlo simulation. The results are determined using the parameters in Tables 3 and 4. These values are characteristic of a stainless steel. The results are compared with trends in the experimental data from the literature. The comparisons show that the small crack growth model is able to predict the significant aspects of small crack growth behavior.

One aspect of small crack growth behavior is that the average crack growth rate is much higher than what would be predicted based on long crack growth data and

applied ΔK. Figure 19 shows experimental crack growth rate data for small cracks from Phillips and Newman [112]. (The curves are re-plotted from the data in Fig. 3 of [112] for an aluminum alloy.) Figure 19 shows that, not only do small cracks grow much faster than ΔK equivalent long cracks, but that da/dN versus ΔK is a function of the applied stress. Thus, ΔK based similitude is not valid for small crack growth.

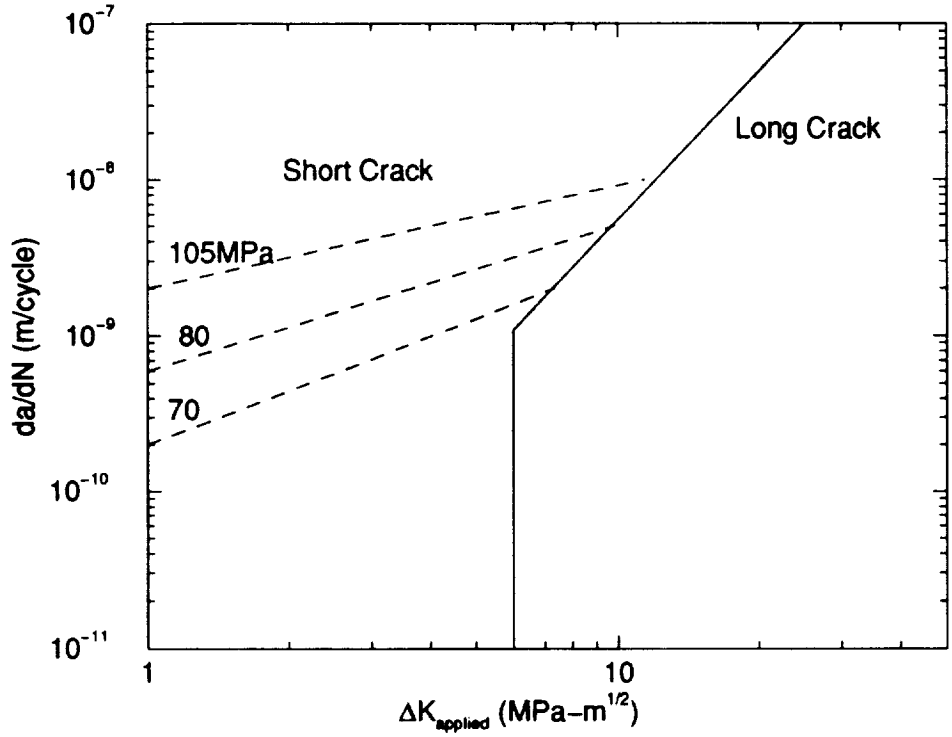

Figure 19: Applied stress effect on crack growth rate (data from Phillips and Newman).

Figure 20 shows the predicted average crack growth rate as a function of applied ΔK. The results compare favorably with experimental results of Phillips and Newman.

Another aspect of small crack growth behavior is that the mean crack growth rate for coarse grain microstructures is higher than the crack growth rate for fine

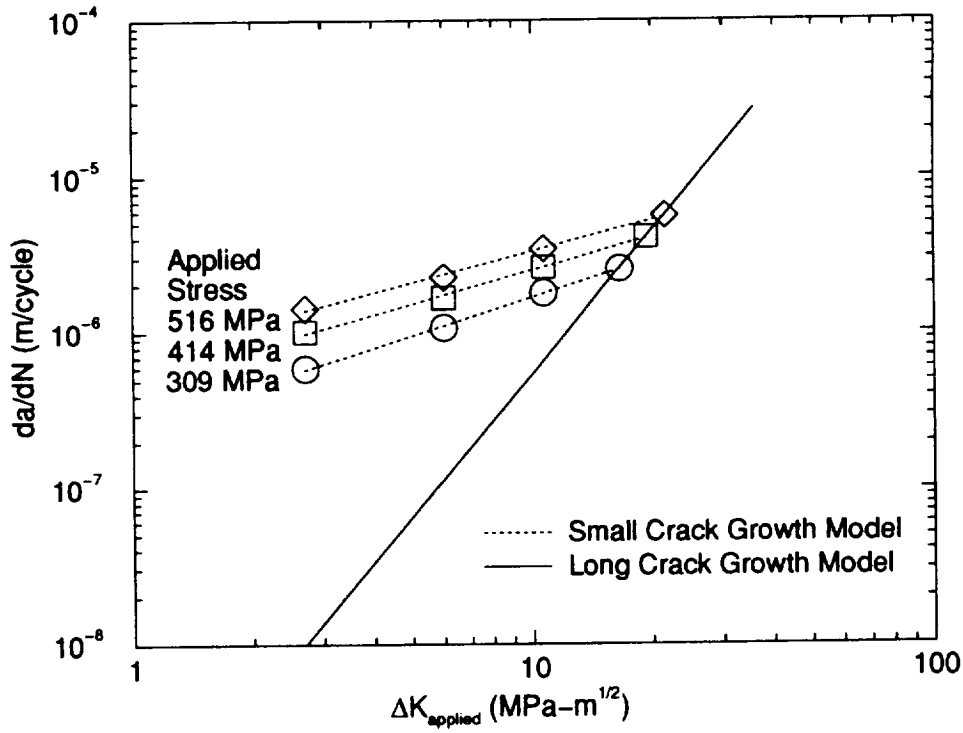

Figure 20: Predicted applied stress effect on crack growth rate.

grain microstructures of the same alloy [59, 113]. This is in contrast to long crack growth rate behavior which shows that, in general, the crack growth rate for coarse grain microstructures is lower than fine grain microstructures. These observations are significant because the assumption has been made, based on long crack growth data, that the coarse grain materials produce better fatigue resistance. However, for cracking in service application, the small crack growth regime must be considered. The overall fatigue resistance may be driven by the small crack growth behavior [114].

Figure 21 shows the predicted average crack growth rate for two microstructures in which the average grain size has been changed. The figure shows that the crack growth rate is lower for the fine grain microstructure. In small cracks, the low growth rate for fine grain microstructures is attributed to the fact that there are more grain boundaries available to retard crack growth than what would be available over the

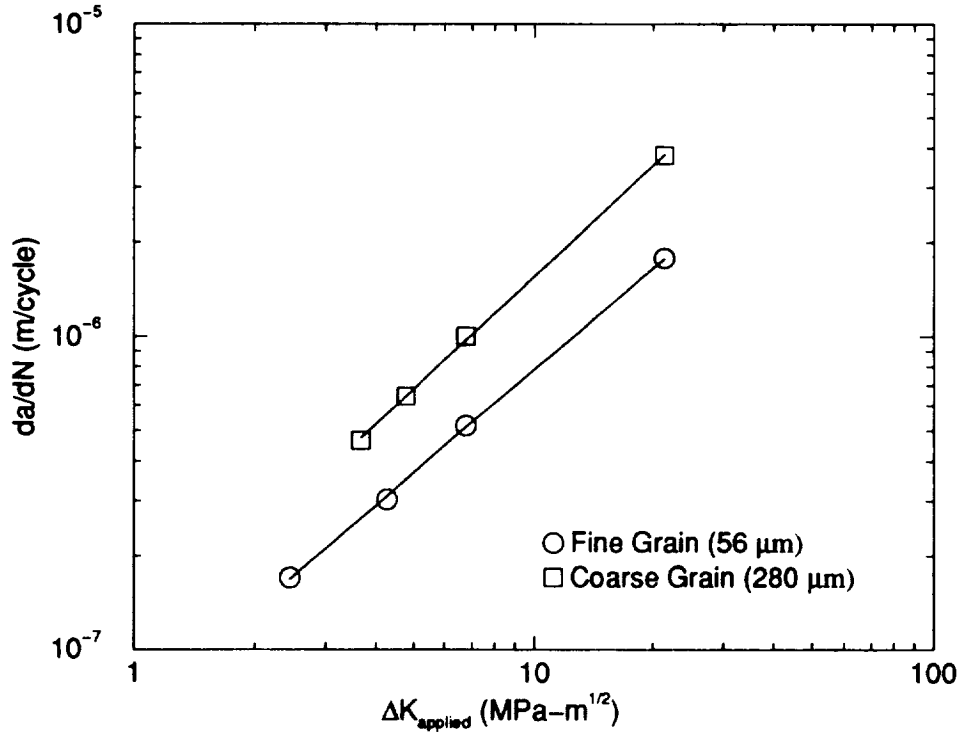

Figure 21: Predicted average grain size effect on small crack growth rate.

same distance in a coarse microstructure. The difference in long crack growth rate for different grain size microstructures is attributed to two factors: closure and intergranular (grain boundary) cracking. The fine grain material has a smoother fracture surface allowing for less opposing crack face roughness induced closure [63]. An element of intergranular cracking is observed as the plastic zone becomes large compared the the grain size [115]. Intergranular crack growth rates are generally higher than transgranular [116]. The introduction of the intergranular cracking will take place at a lower ΔK for the fine grain material. A combination of less closure and more intergranular cracking causes a reduction in the overall fatigue resistance for the fine grain material.

Figure 22 shows the predicted crack growth rate as a function of crack length for 5 cracks that have successfully penetrated the first grain boundary. The crack growth

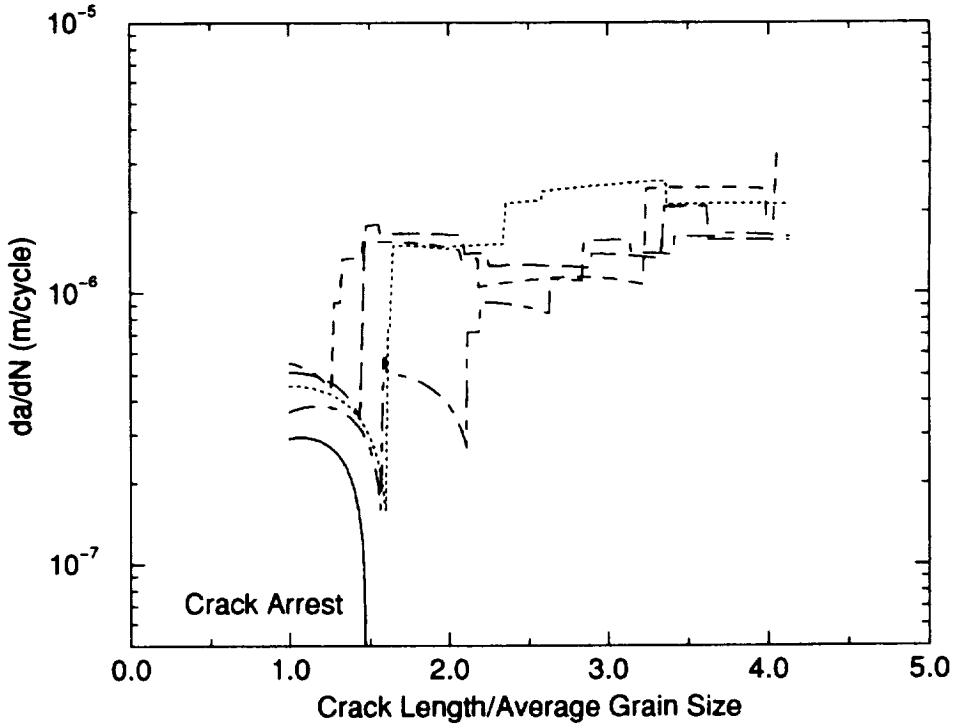

Figure 22: Predicted small crack growth behavior for five cracks during low stress high cycle fatigue.

rate seems to vary haphazardly as the crack interacts with the microstructure. Similar behavior has been observed experimentally by many investigators [117, 118, 119, 120]. The only obvious correlation that has been made between the crack growth rate and the microstructure is that the large jumps in crack growth rate can be associated with the crack tip nearing the grain boundary.

The small crack growth equations 42 through 46 indicate that several factors govern the interaction between the crack growth rate and the microstructure.

- The crack length.
- The local effective resolved shear stress at the crack tip.
- The local effective frictional stress at the crack tip.

- The slip band length.

- The effective resolved shear stress along the slip band.

- The effective frictional stress along the slip band.

- If the slip band tip is propagating or blocked.

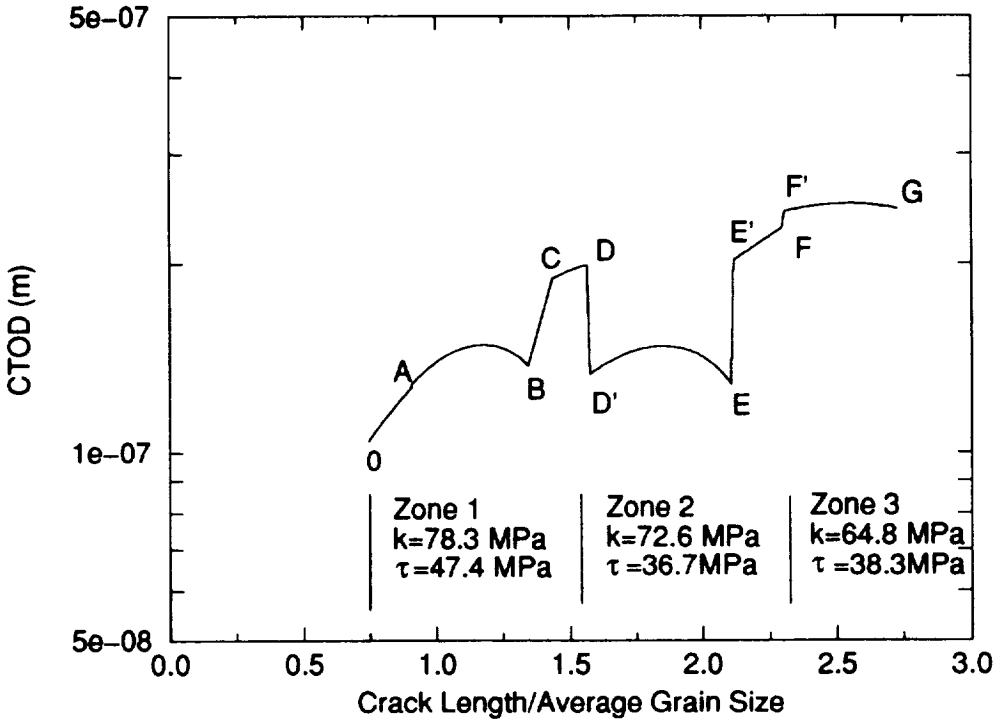

Figure 23: Predicted small crack growth behavior for one cracks during low stress high cycle fatigue.

To illustrate these interactions, consider the predicted small crack growth rate versus crack length curve for a single crack chosen at random shown in Fig. 23. Grain boundaries are located at O, D, and F. The average frictional stress is $70MPa$. The average resolved shear stress is $41.4MPa$. The local effective properties are shown in the figure. The following list describes the conditions governing crack growth for the various regimes in Fig. 23:

- *Crack tip between O and A.* The crack tip is in zone 1. The slip band tip is propagating in zone 1.

- *Crack tip between A and B.* The crack tip is in zone 1. The slip band tip is blocked at the boundary between zones 1 and 2.

- *Crack tip between B and C.* The crack tip is in zone 1. The slip band tip is propagating in zone 2.

- *Crack tip between C and D.* The crack tip is in zone 1. The slip band tip is blocked at the boundary between zones 2 and 3.

- *Crack tip between D′ and E.* The crack tip is in zone 2. The slip band tip is blocked at the boundary between zones 2 and 3.

- *Crack tip between E′ and F.* The crack tip is in zone 2. The slip band tip is blocked at the boundary between zones 3 and 4.

- *Crack tip between F′ and G.* The crack tip is in zone 3. The slip band tip is blocked at the boundary between zones 3 and 4.

As the crack grows the slip band becomes large and spans several grain. The crack continues to grow in such a manner until the effective properties of the material between the crack tip and the slip band tip approach the bulk properties.

Figure 24 shows the small crack growth behavior at high stress low cycle fatigue. The low cycle fatigue has a large slip band length which spans many grains. The slip band experiences near average properties even when the crack is very small. Thus, the scatter in the low cycle fatigue crack growth rate is significantly less than the high cycle fatigue crack growth rate.

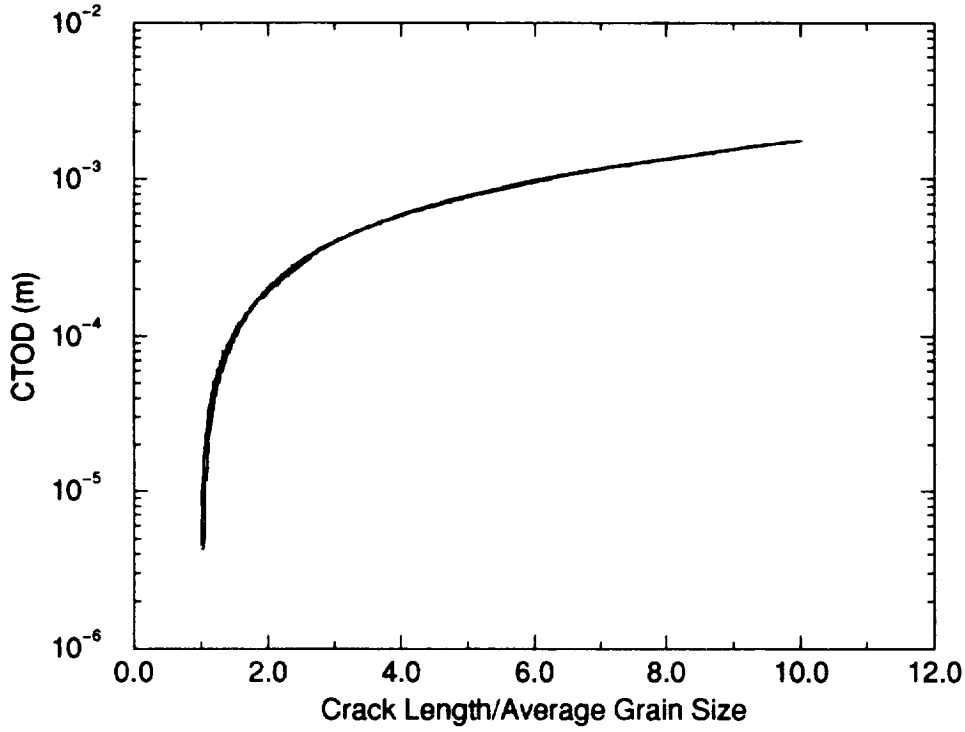

Figure 24: Predicted small crack growth behavior for high stress low cycle fatigue.

Variable	Value	Description
d_{avg}	$55.8\mu m$	Average Grain Diameter
G	$76 \times 10^3 MPa$	Bulk Shear Modulus
k_{avg}	$69MPa$	Bulk Frictional Stress
ν	0.3	Poisson's Ratio
W_s	$440kN/m$	Specific Fracture Energy
C_{avg}	$4.4 \times 10^{-9} MPa\sqrt{m}$	Average Paris Law Coefficient
n	3	Paris Law Exponent
β'	0.1	CTOD Law Coefficient
K^M_{crit}	$769MPa\sqrt{m}$	Critical Microscopic Stress Intensity Factor
da	0.5	Crack Growth Law Interval

Table 5: Deterministic parameters for reliability analysis.

Predicted Total Fatigue Life of a Test Specimen

It is difficult to compare the probabilistic model predictions for total fatigue life directly with experimental data because the parameters used in the model are usually not reported. However, the predicted scatter in fatigue data is compared with trends in the experimental data and the predicted mean life for different size specimens is compared with size effect observations.

The distribution of fatigue life for the individual grains is shown in Fig. 25. This distribution was determined using the parameters in Tables 3 and 5 in a Monte Carlo analysis. These values are characteristic of a stainless steel.

The analysis produce a mean fatigue life of 265,000 cycles with a very heavy upper tail as shown in Fig. 25. The distribution of fatigue life appear to be lognormal. Plotting the distribution on lognormal paper in Fig. 26 indicates that the lognormal distribution may not be a good fit (correlation coefficient $R = 0.972$). The heavy tail causes the curve to bend to the right. (A lognormal distribution would plot as a straight line on lognormal paper with $R = 1$.) The distribution cannot be directly compared to experimental data because no data exist on the fatigue life of cracks initiating in each grain of a test specimen. The specimen fails when a single crack grows to final fracture.

The distribution of fatigue life for test specimens was predicted by assuming the specimen has a circular cross section with radius $7.62mm$, and a shallow notch with a gauge surface area of $1.61mm^2$. This gauge surface area results in about 4000 grains per specimen. Different specimens will have a different number of surface grains and therefore the number of surface grains is a random variable. The predicted PDF of fatigue life for the specimens is shown in Figure 27. The mean life of the specimens

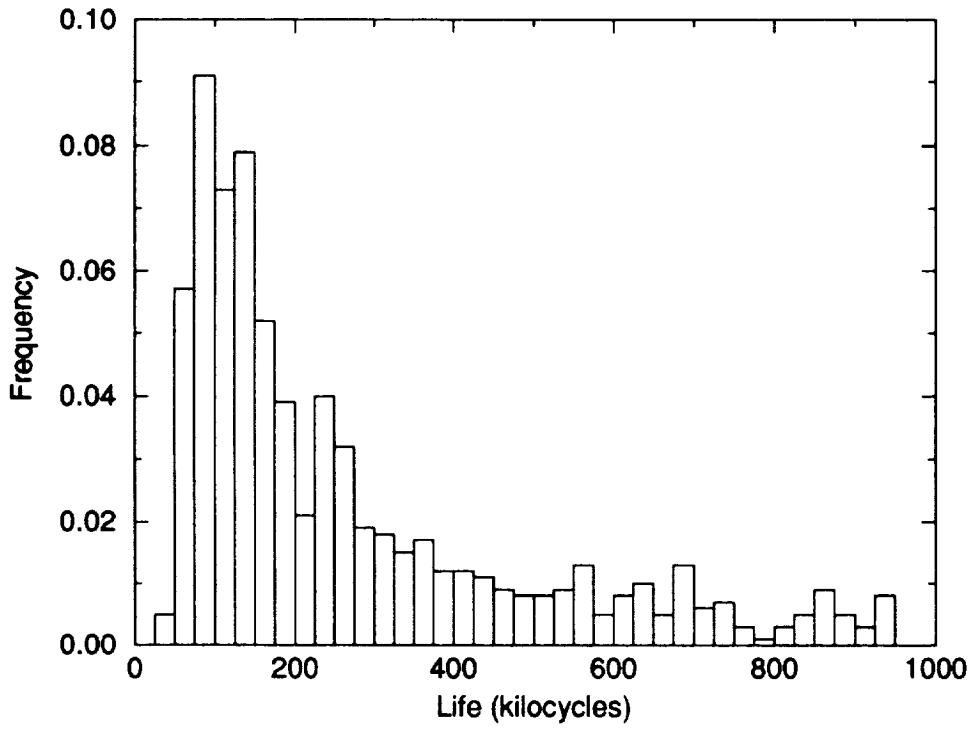

Figure 25: Fatigue life distribution of the individual grains in a specimen.

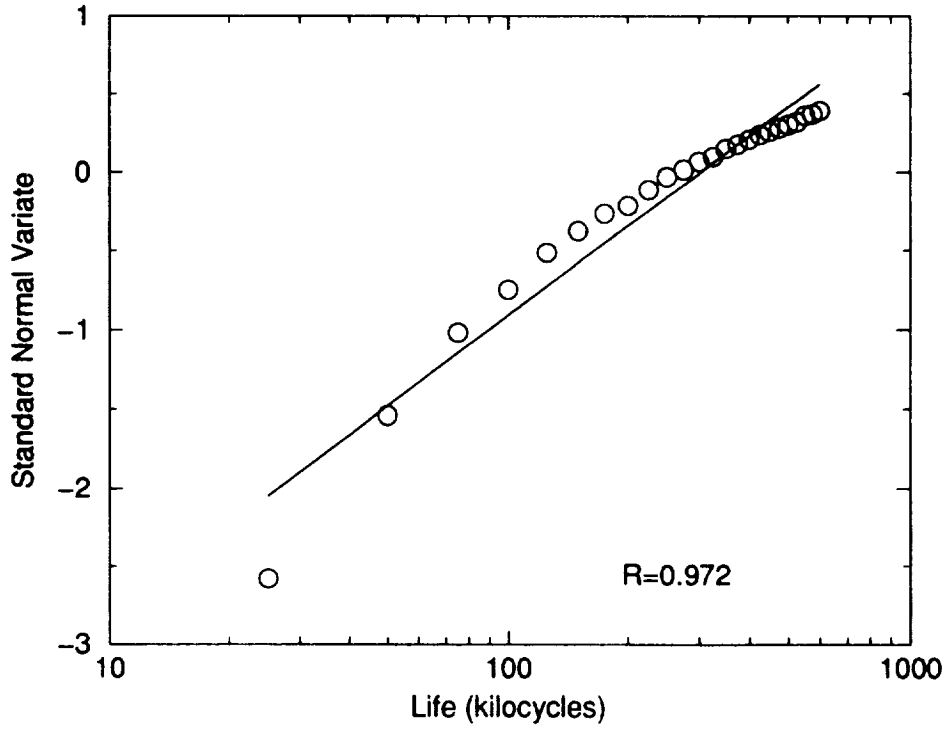

Figure 26: Fatigue life distribution of the individual grains in a specimens plotted on lognormal probability paper.

is 60,000 cycles with a COV of 0.17.

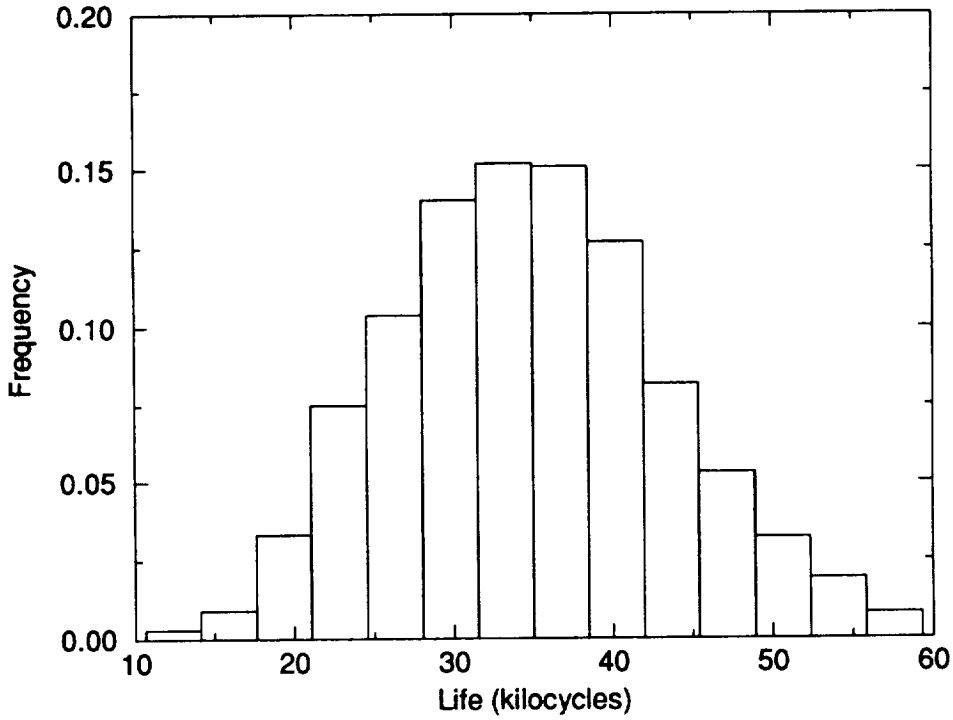

Figure 27: Fatigue life distribution of the specimens

Figure 28 shows that fitting the model results to a lognormal distribution gives a correlation coefficient of 0.993. Fitting the model results to a normal distribution in Fig. 29 gives a correlation coefficient of 0.999. Both the normal and lognormal distributions provide an adequate representation of the model results and both have been used to represent experimental data [3][22, pp. 380].

The distribution of the number of cycles spent in the crack nucleation, small crack growth, and long crack growth stages is shown in Figs. 30, 31, and 32 respectively.

A thorough investigation of the scatter in fatigue life is not available in the literature for most alloys. Many manufacturers, particularly in the aerospace and nuclear industries, have the large compilation of data used for statistical characterization. But, the cost associated with such test is considerable and the data is tightly held.

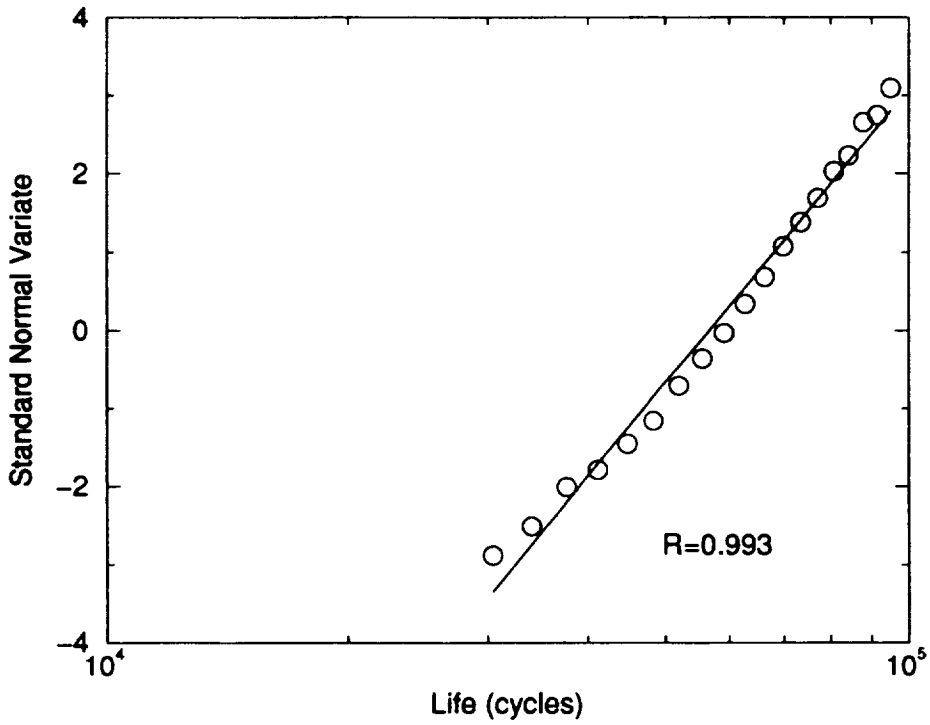

Figure 28: Fatigue life distribution of the specimens plotted on lognormal probability paper.

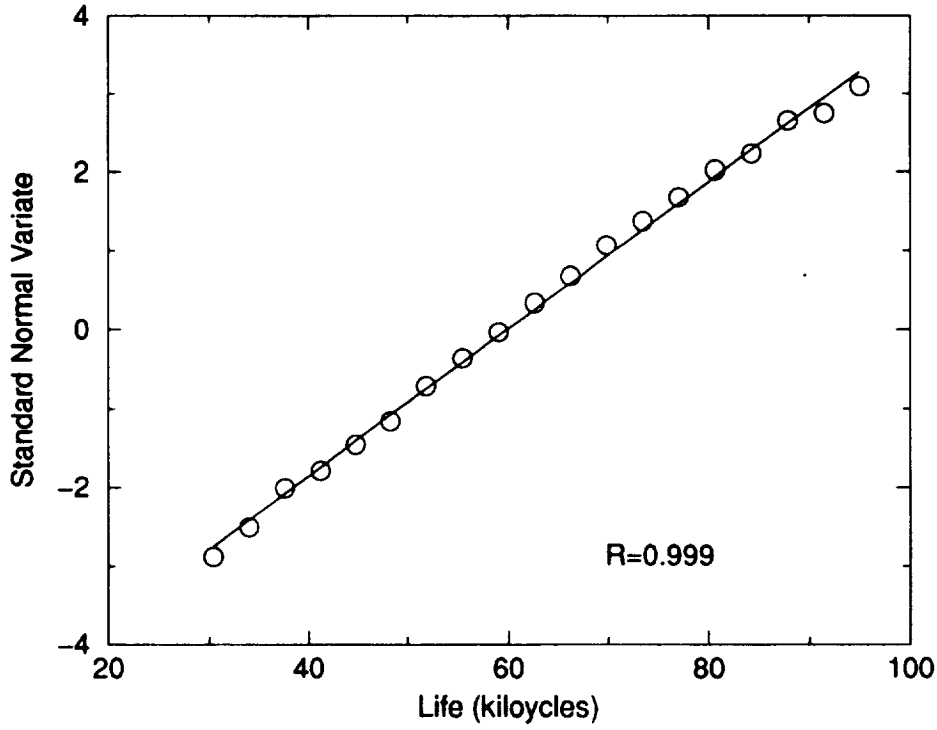

Figure 29: Fatigue life distribution of the specimens plotted on normal probability paper

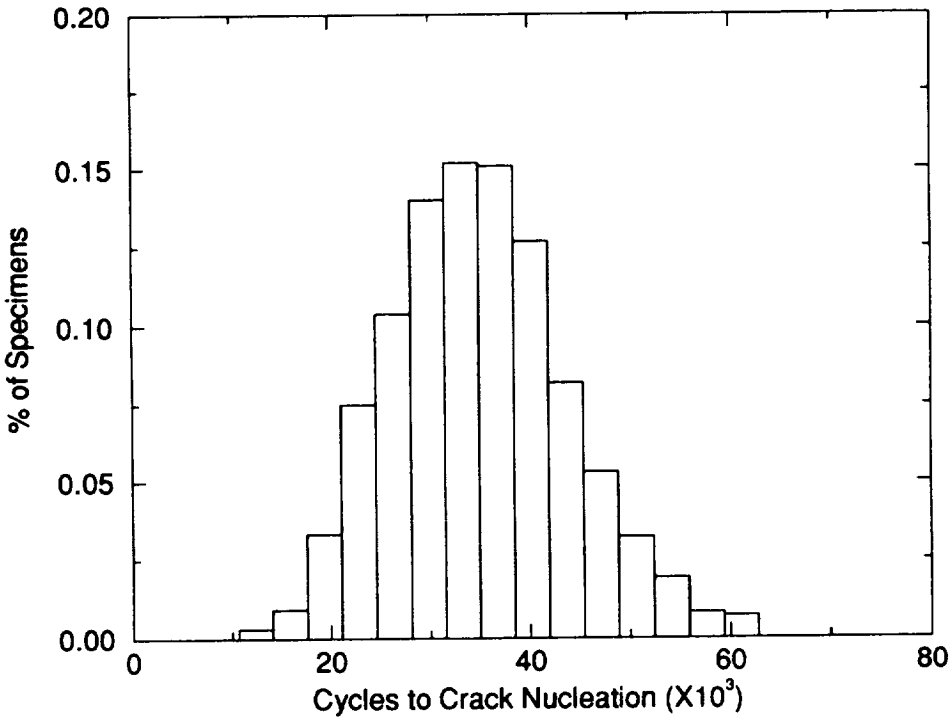

Figure 30: Distribution of cycles spent in the crack nucleation stage

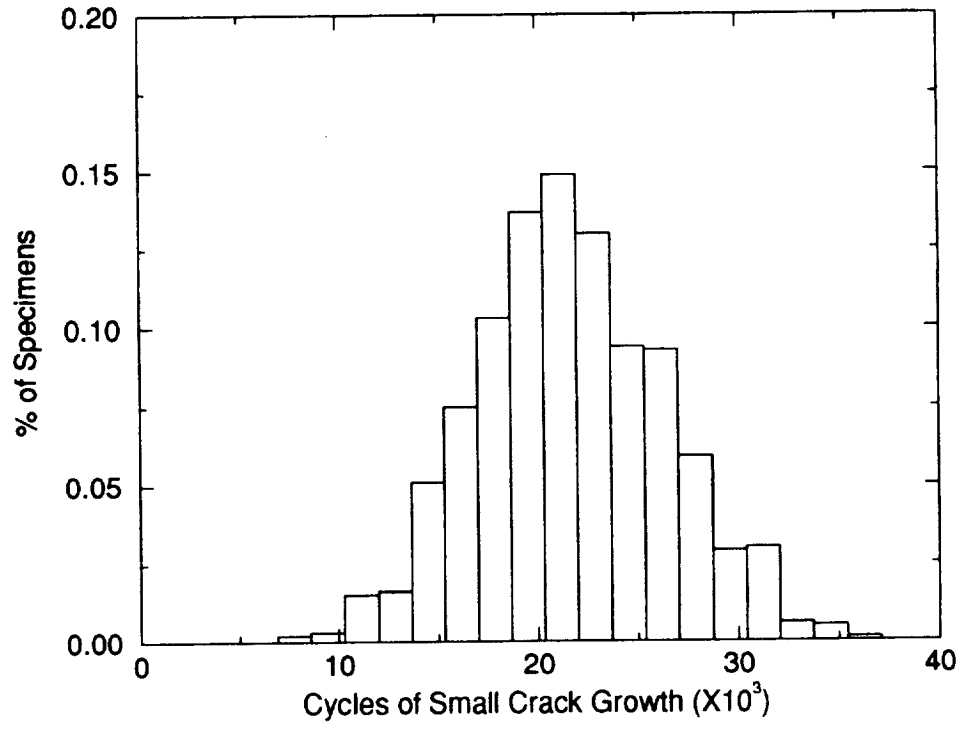

Figure 31: Distribution of cycles spent in the small crack growth stage

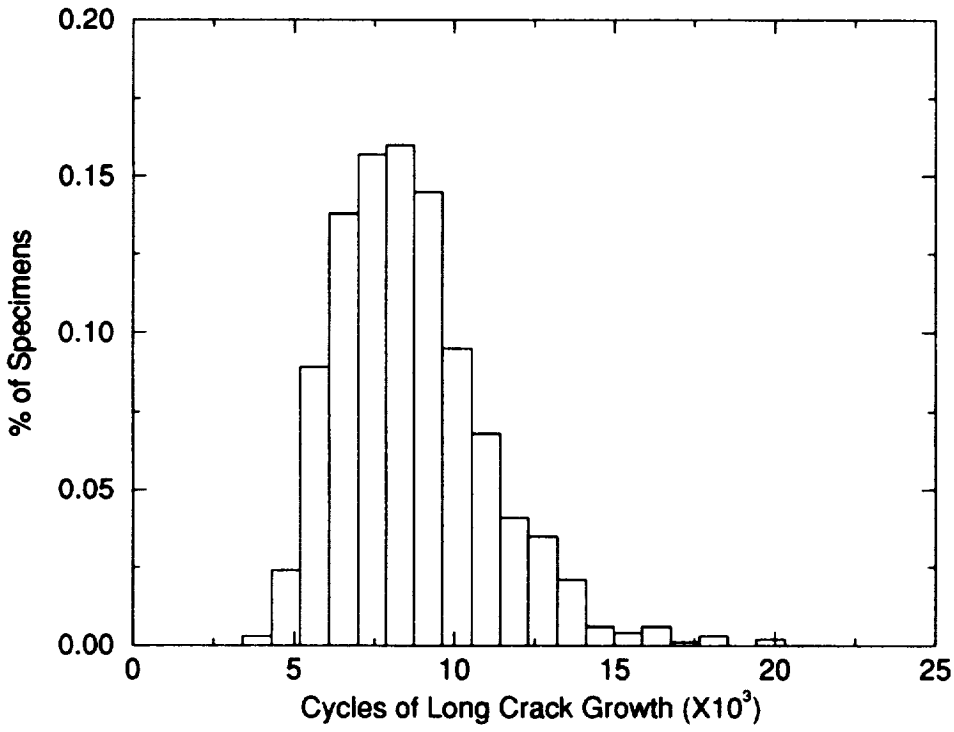

Figure 32: Distribution of cycles spent in the long crack growth stage

However, Bastenaire [3] performed a thorough investigation of the scatter in fatigue life for five different grades of low alloy steel.

Steels may nucleate cracks by mechanisms other than slip band cracking depending on the alloy composition and the impurities. However, the trend in the scatter in steel data has been observed in other metallic alloys [2]. Bastenaire performed rotating bending fatigue experiments for many stress levels for each grade of steel with several hundred specimens for each stress level.

Figure 33 shows the trends in the scatter exhibited in Bastenaire's data. (The curves are re-plotted from the data in Fig. 7 of [3].) The general trend is that the COV (indicated by the slope of the curves) is fairy constant for applied stresses well above the fatigue limit (363-324 MPa). As the applied stress decreases, the COV starts to increase (304-285 MPa). As the applied stress approaches the fatigue limit,

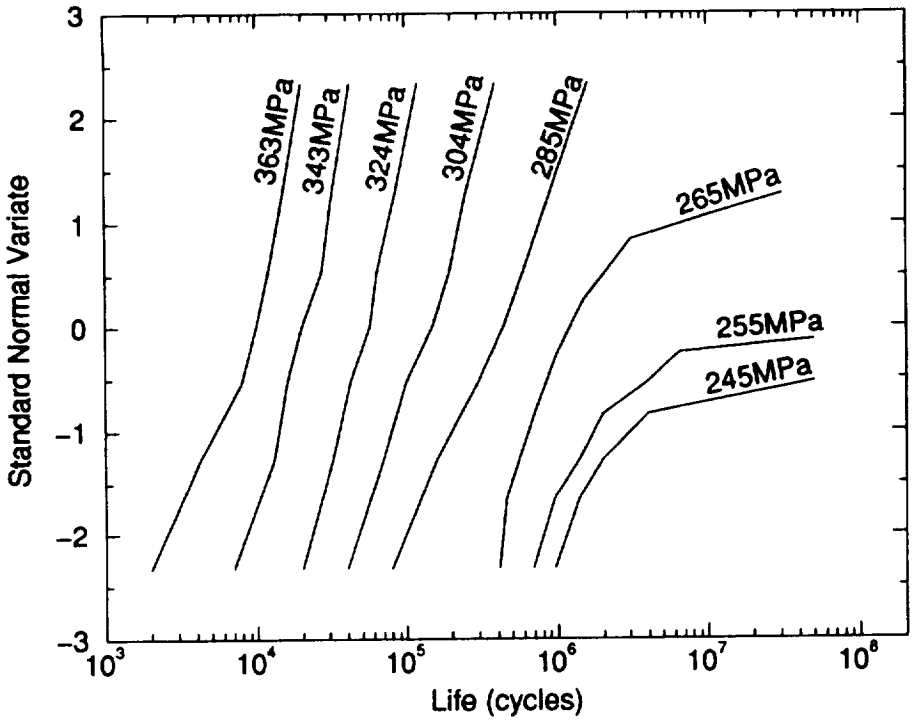

Figure 33: Fatigue life test data plotted on lognormal paper (data from Bastenaire).

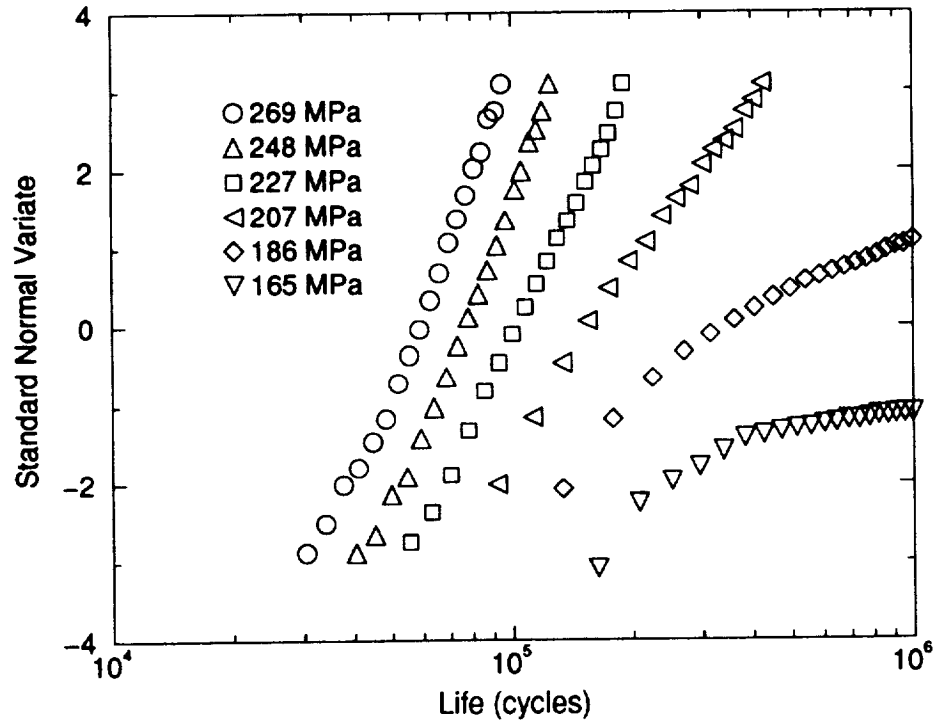

Figure 34: Predicted fatigue life distribution plotted on lognormal paper.

run-outs start to occur. The right tail of the distribution becomes heavy which causes a line through the data to bend to the right (265-245 MPa). If data plots as a non-straight line in Fig. 33 the lognormal distribution is no longer valid. The 363 MPa data curves slightly to the left indicating the distribution has a short right tail and the data can also be fitted to the normal distribution. As the applied stress decreases, the curvature shifts to the right.

Comparison of Fig. 33 with the results in Fig. 34 shows that the model predicts all of the above trends observed in the experimental data. Fig. 35 presents the same data in the familiar form of a SN diagram. The runouts (suspensions) are the percentage of specimens that did not fail at 10^6 cycles.

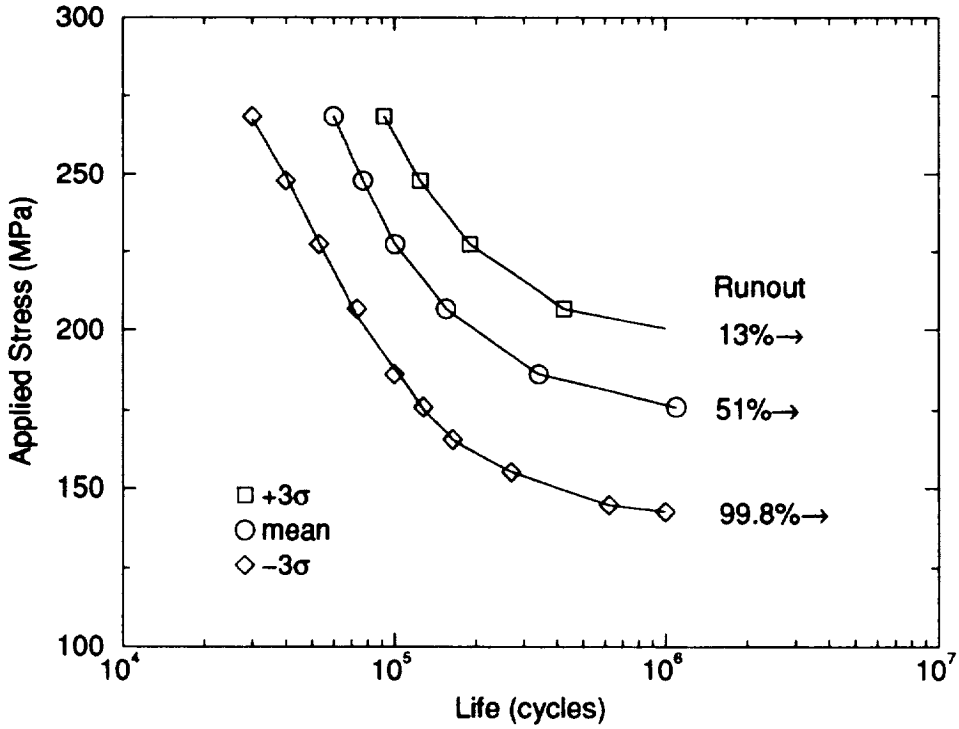

Figure 35: Predicted stress versus life curve.

Nishijima *et al.* [121, 122] showed the fatigue strength distribution to be normal for various steels as shown in Fig 36. (The curves are re-plotted from the data in

Fig. 4 of [121] for a low carbon steel.) This observation has been made in other alloys [22]. Comparison of Fig. 36 with the results in Fig. 37 shows that the model predicts similar behavior.

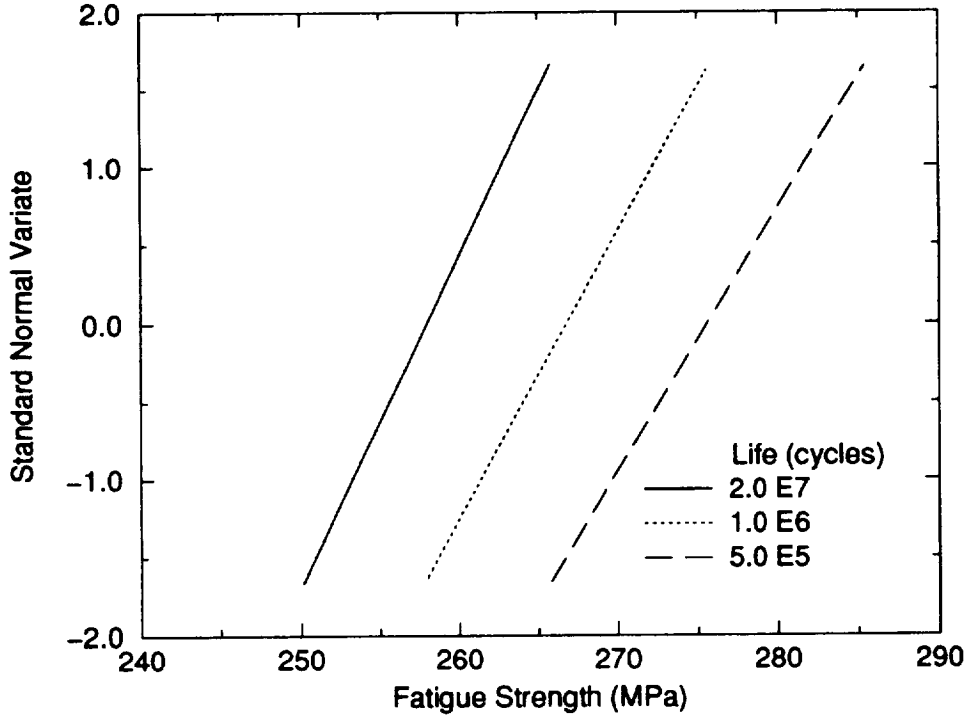

Figure 36: Fatigue strength data plotted on normal paper (data from Nishijima *et al.*).

The Monte Carlo simulation showed that most of the failures were caused by the largest grain in the specimen and almost all the failures were initiated in one of the 5 largest grains. The lower the stress the more failures initiated in the largest grain. This indicates that the "weak links" in crack nucleation are the largest grains. Experimental evidence shows that failures can be associated with the largest grains [12, 31].

The distribution of the largest defects (or the largest grains in the present model) lead to the size effect model developed by Weibull [123]. Size effect is the phenomenon that small components have a higher fatigue life than larger geometrically similar

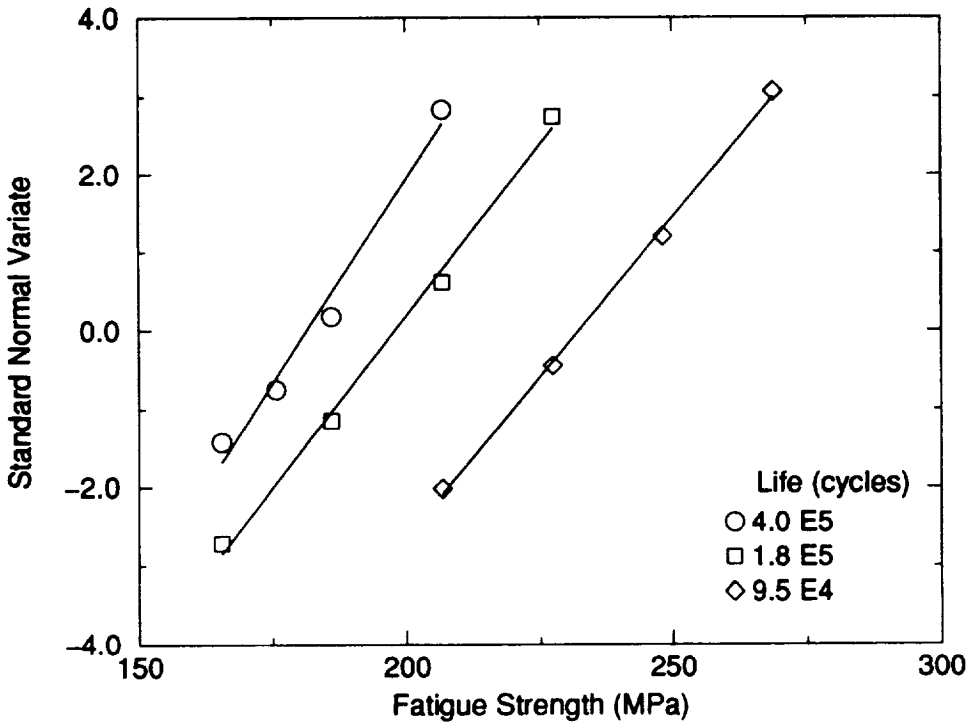

Figure 37: Predicted fatigue strength plotted on normal paper.

components. Weibull assumed that the larger component is more likely to have a larger life controlling defect. This approach is widely used in the design of ceramics and it has also been applied to ductile materials [124].

The reliability of different size (defined by the mean number of surface grains) specimens was determined and the mean fatigue strength at an arbitrary life is plotted against size in Fig. 38. The model indicates that very large structures have zero life. This is because a lognormal distribution of grains allows an infinitely large grain in a infinite population. In reality, the grain size cannot be infinite and the true distribution of grain size is truncated as discussed in Chapter VI. The fatigue life of a very large structure would be controlled by this maximum truncated grain size.

The predicted size effect on fatigue strength is linear in log space as shown in Fig. 38. The same relationship was predicted analytically by Trantina [124] using a

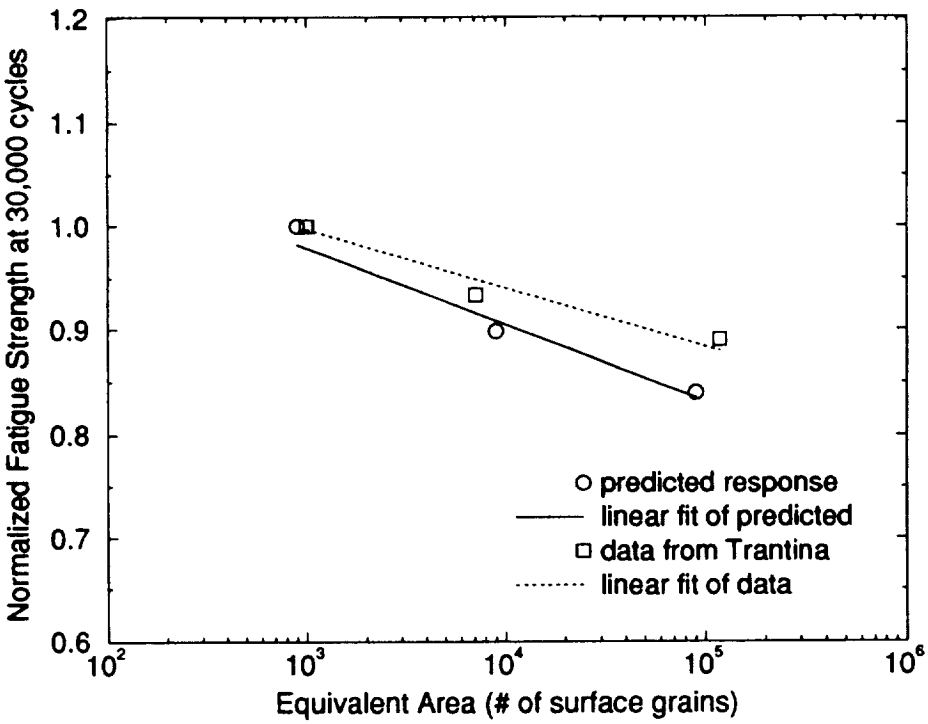

Figure 38: Predicted mean fatigue life for various size specimens.

weakest link theory. The experimental observations on smooth, bolt hole, and sharp notched specimens which Trantina used to validate his predictions have been scaled with respect to fatigue strength for comparison with the model predictions in Fig. 38. The data exhibited is for a different material than that modeled, therefore, a direct comparison cannot be made. The important point demonstrated by Fig. 38 is that the model predicts that the fatigue life decreases linearly with an increased in the log of volume (or surface area). The intercept of the line depends on the specified fatigue life. The slope of the line, which represents the sensitivity of the material to size effect, depends on the scatter of the fatigue strength controlling variables and can vary with material processing and material alloy [124].

Sensitivity of Total Fatigue Life to the Random Variables

The sensitivities shown in Fig. 39 represent the sensitivity of the total fatigue life COV to the random variable COV

$$\frac{\%\text{ change in total life COV}}{\%\text{ change in random variable COV}} \tag{62}$$

A Monte Carlo simulation was performed using the nominal variations in Table 3. Then a separate Monte Carlo simulation was performed for each of the random variables in which the COV the random variable was decrease by 5%. The sensitivities have been normalized such that the summation of sensitivities is 1.

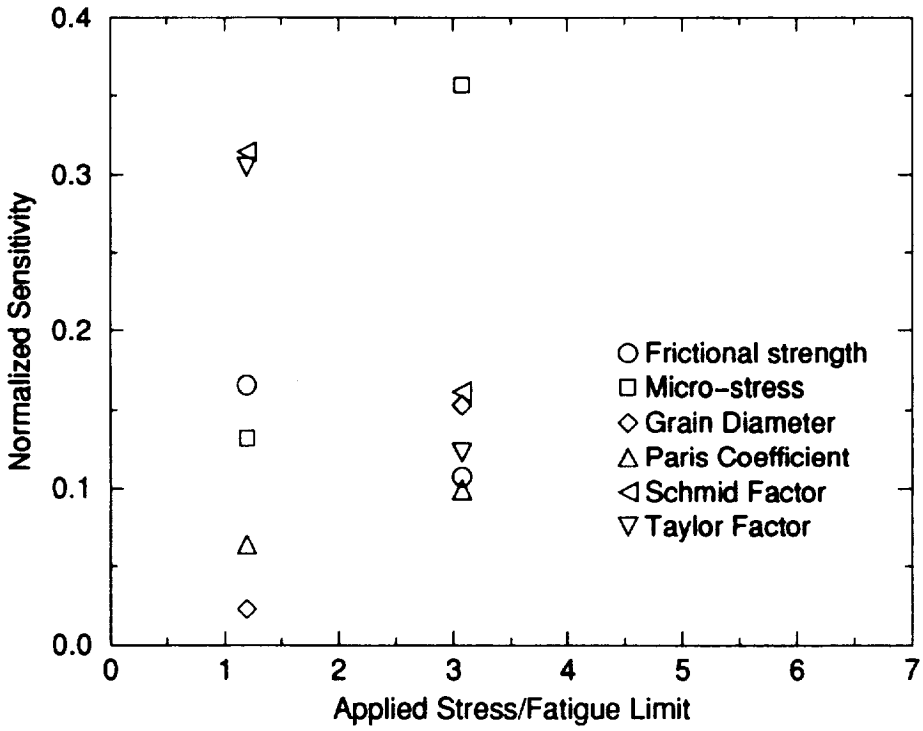

Figure 39: Importance of the random variable variation on the fatigue life variation.

Figure 39 shows that at low stress (high cycle fatigue), the variation in fatigue life is most sensitive to the variation in the grain orientation. It is well known that texturing can greatly effect high cycle fatigue life. The variation in high cycle fatigue

life is shown to be least sensitive to the variation in grain size. The Monte Carlo simulation showed that at low stress, the largest grains were responsible for the failure causing crack. It would seem that the fatigue life would be sensitive to the grain size distribution. However, the distribution of the largest grains in each specimen is an extreme–value distribution and will only change slightly with a 5% decrease in the COV of grain size for all of the grains in the specimen.

Figure 39 show that at high stress (low cycle fatigue), the variation in fatigue life is most sensitive in the variation in the applied microstress. In low cycle fatigue the crack tip plastic zone is large and not as sensitive to the local material property variations. The scatter in fatigue life is more sensitivity to grain size variations in low cycle fatigue than in high cycle. This is because the failure causing crack is less likely to be associated with the largest grain in the specimen. The grain size distribution for all of the grains in the specimen will better characterize the distribution of grains associated with the failure causing cracks in low cycle fatigue than in high cycle fatigue.

Reductions in the fatigue life COV could be realized by reducing the scatter in the random variables. The grain size distribution for cast materials is controlled by the well behaved kinetics of normal grain growth and invariant to most parameters. Specialized metallurgical processes have been developed to specificly control the variation in grain size. Rhimes and Patterson [125] were able to control the COV of the grain volume distribution for forged alloys by the degree of cold working before annealing. They were able to change the COV many fold through careful processing. Kozaczek *et al.* [94] found that the COV of the micro-stress distribution was controlled by the elastic anisotropy of the material, which can be changed through material alloying.

Grain orientation distribution is effect by forming processes such as forging, drawing, and stamping. No reliable data exist on the controlling factors for the frictional stress distribution. It would be reasonable to assume that impurities effect the frictional shear stress, and that reducing impurities would reduce the variation in frictional stress.

CHAPTER IX

SUMMARY AND CONCLUSIONS

This study develops a probabilistic mesomechanical approach to relate the variation in the material microstructure to the variation in the fatigue life of macrostructural components. The study investigates the regimes in which the effects of the local variation in the microstructure are assumed to be dominant: crack nucleation and small crack growth. The purpose of the study is to investigate only the microstructural effects. Variations in the applied loading, stress concentrations, residual stresses, and global geometry are not considered.

The components modeled are single phase polycrystals. The grain shape is assumed to be equiaxial and the grain orientation is untextured and described using the $\{110\}\langle 111\rangle$ slip system. The loading and material properties within a grain are homogeneous although not isotropic. The loading and material properties vary from grain to grain. The component geometries are simple smooth test specimens.

The fatigue process is divided into three phases. The first phase is the crack nucleation phase. The theory of continuously distributed dislocations is used to model the persistent slip band within a grain. Dislocations pile up at the grain boundaries with each load cycle. When the energy associated with the dislocation pile-up exceeds a critical value, a crack forms along the slip band the size of the grain.

The second phase is the small crack growth phase. The crack growth rate is modeled as a function of the crack tip opening displacement (CTOD). The theory of continuously distributed dislocations is used to model the CTOD. The plastic zone

is modeled as dislocations distributed ahead of the crack tip. The tip of the plastic zone can either be propagating freely within a grain or blocked at the grain boundary. The CTOD depends on the relative location of the crack tip and the plastic zone tip. The crack grows in the small crack growth phase until the plastic zone spans many grains so that local variations have little effect.

The local microstructural variables considered random are: grain size, grain orientation, micro-stress, and frictional stress. The variables are common to both the crack nucleation and small crack growth models.

The third phase is the long crack growth phase. The crack growth rate is modeled using Paris law. The microstructural variations are not explicitly considered. All variation in long crack growth is model by allowing the Paris law coefficient to be a random variable.

The model predicted many aspects of fatigue observed in the experimental data. These include:

- The shape of the crack nucleation life distribution
- The applied global stress effects and the mean grain size effect on the COV of crack nucleation life.
- The applied global stress effects and the mean grain size effect on small crack growth rate.
- The variation in small crack growth rate.
- The shape of the total fatigue life distribution.
- The applied global stress effects on the shape of the total fatigue life distribution.

- The knee in the SN curve and run-outs

- Multiple cracks

- The size effect

This study demonstrates the feasibility of developing probabilistic mesomechanical material models which can link the variation in the material microstructure to the scatter in fatigue life. The benefits of such a model are two fold.

1. The models will allow the structural engineer to systematically and quantitatively assess the influence of the material uncertainties on the overall reliability of the structure.

2. The models can be developed concurrently with material development to identify the sources of uncertainty. Material testing can be tailored to measure the most important source of uncertainty. The material engineer can then design the material to minimize the scatter thus increasing the useful properties.

CHAPTER X

FUTURE RESEARCH

Model Validation

The use of probabilistic mesomechanics to determine the fatigue behavior of a test specimen was illustrated. A complete set of the experimental data needed to define the random variable distributions was not available for a individual alloy. Data from a variety of alloys was used and therefore the model results could only be compared with general trends in the observed fatigue behavior. The proposed method requires experimental validation on an individual alloy. The alloy should be a low stacking fault, single phase alloys such as a nickel or austenitic steel and be free of crack nucleating inclusions.

The direct experimental techniques available for validating micromechanical crack nucleation and small crack growth models are discussed by Bailon and Antolovich [126]. Many other useful experimental techniques are given in the literature [127, 128, 129, 130].

Large Components

The proposed model is only valid for simple geometric specimens. For the model to be applied to real engineering structures such as crack shafts or turbine blades, statistical and physical correlation issues must be addressed.

The controlling random variables may be spatially correlated within the various

mesodomains for individual large components. For example, the distributions describing the material microstructure in the airfoil and dovetail regions of a single fan blade will be physically correlated because each location experiences the same heat treatment history while the forging flows are different for each. Damage accumulation response is correlated within and between mesodomains because the entire component experiences the same service history. However, the dynamic load conditions for different locations on the structure are fully correlated. For example, the airfoil loading may be dominated by forced aerodynamic loading at high frequencies, and relatively small mean stresses. The blade root stresses will be dominated by engine centrifugal loadings.

The fatigue model has to consider the spatial correlations between the different physical variables or material properties. For this reason, these quantities have to be modeled as random fields. Each random field is modeled as discrete random variables, such that each random variable represents the statistical quantity over a particular spatial region. Since all these random variables are derived from the same random field, they are correlated to each other, based on their mutual distance. Simple exponential and triangular models [131] have been proposed in the literature to describe such correlation structure. Another method for the efficient discretization of a random field, based on its correlation structure and its influence on the structural response of interest, is given in [132].

Composite Structures

The necessity of a probabilistic approach to microstructural modeling in determining the mechanical properties of materials is not limited to metallic structures.

The need to increase the thrust to weight ratio of current propulsion systems has lead to an emerging technology in advanced materials. The goal of this technology is to develop light weight structures able to withstand high temperatures. Several materials with low density, high strength and high temperature capability have been identified such as metal matrix composites and ceramic matrix composites. Composite behavior is driven by the microstructure which is highly inhomogeneous. The mechanical response of composite materials has more apparent scatter than metallic structures.

Whereas mechanical responses such as creep and large crack propagation have been successfully modeled for many metallic application based on macrostructural parameters, the response of composites cannot be modeled in this manner. Creep experiences matrix-fiber debonding and fiber pull-out. Crack growth is compound by fiber bridging. Crack initiation is influenced by the cross weave structure. All of these issues are random in nature and contribute to the increased scatter seen in the behavior of composite materials. The large scatter decreases the minimum material properties which severely limits the use of such materials, especially due to their lack of toughness.

The behavior of structures composed of composite materials must be determined using models that account for the complexities inherent in composite microstructures. Models are needed for composite materials that relate overall stress, strain, temperature and environment to crack nucleation, crack growth, and creep. These models must account for such microstructural parameters as matrix strength, fiber strength, fiber density, cross weave fibers, fiber-matrix interaction and residual processing stresses. A probabilistic mesomechanical approach is necessary to understand

the mechanical behavior of such complex materials.

Composite material test technology is still in its infancy. Test equipment and procedures are currently being designed to support the data acquisition necessary for a rudimentary understanding of damage accumulation and failure [133]. Development of probabilistic mesomechanical models will help guide the design of test procedures and techniques that support the data acquisition necessary to identify the important sources of uncertainty.

BIBLIOGRAPHY

[1] Tryon, R. G., Cruse, T. A., Mahadevan, S., "Development of a Reliability-Based Fatigue Life Model for Gas Turbine Engine Structures", Engr. Frac. Mech., Vol 53, No. 3, pp. 807-828, 1996.

[2] Sasaki, S., Ochi, Y., Ishii, A., Hirofumi, A., "Effects of Material Structures on Statistical Scatter in Initiation and Growth Lives of Surface Cracks and Failure Life in Fatigue", JSME Inter. J., Series I, Vol. 32, No. 1, pp. 155-161, 1989.

[3] Bastenaire, F. A., "New Method for the Statistical Evaluation of Constant Stress Amplitude Fatigue-Test Results", *Probabilistic Aspects of Fatigue*, Ed., Heller, R. A., ASTM STP 511, pp. 3-28, 1972.

[4] Halford, G. R., "Evolution of Creep-Fatigue Life Prediction Models", *Creep-Fatigue Interactions at High Temperatures, AD-Vol. 21*, Ed., Haritos, G. K., Ochoa, O. O., ASME, pp. 43-57, 1991.

[5] Schijve, J., "Fatigue Predictions and Scatter", Fat. Fract. Eng. Mat. Struct., Vol. 17, No. 4, pp. 381-396, 1994.

[6] R. E. Little and E. H. Jebe, *Statistical Design of Fatigue Experiments*, Applied Science Publ., Essex U.K., 1975.

[7] Axelrad, D. R., "The Mechanics of Discrete Media", *Continuum Models of Discrete Systems (CMDS3)*, Ed., Kröner, E., Anthony, K.-H., Univ. Waterloo, pp. 3-34, 1980.

[8] Haritos, G. K., Hager, A. K., Salkind, M. J., Wang, A. S. D., "Mesomechanics: The Microstructure-Mechanics Connection", Int. J. Sol. Struct., Vol. 24, No. 11, pp. 1081-1096, 1988.

[9] Nisitani, H., and Takao, K-I, "Significance of Initiation, Propagation and Closure of Microcracks in High Cycle Fatigue of Ductile Metals", Eng. Frac. Mech., Vol. 15, No. 3, pp. 445-456, 1981.

[10] Taira S., Tanaka, K., and Hoshina, M., "Grain Size Effect on Crack Nucleation and Growth in Long-Life Fatigue of Low-Carbon Steel", *Fatigue Mechanisms* ,ASTM STP 675, Ed. Fong, J. T., pp. 135-173, 1979.

[11] Floreen, S., "High Temperature Crack Growth Structure Property Relationships in Nickel Base Superalloys", *Creep-Fatigue-Environment Interactions*, Ed., Pelloux, R., Slotoff, N., Metallurgical Soc., pp. 121-128, 1980.

[12] Tokaji, K., Ogawa, T., Ohya, K., "The Effect of Grain Size on Small Fatigue Crack Growth in Pure Titanium", Fatigue, Vol. 16, pp. 571-578, 1994.

[13] Gayda, J., Miner, R., "Fatigue Crack Initiation and Propagation in Several Nickel-Based Superalloys at 650°C", Int. J. Fat., Vol. 5, No. 3, pp. 135-143, 1983.

[14] Lerch, B., "Microstructural Effects on the Room and Elevated Temperature Low Cycle Fatigue Behavior of Waspaloy", NASA CR 165 497, 1982.

[15] Lankford, J., and Davidson, D. L., "The Role of Metallurgical Factors in Controlling the Growth of Small Fatigue Cracks", *Small Fatigue Cracks*, Ed., Ritchie, R. O. and Lankford, J., The Metallurgical Society, Warrendale, PA, pp. 51-71, 1986.

[16] Bataille, A., Magnin, T., "Surface Damage Accumulation in Low Cycle Fatigue: Physical Analysis and Numerical Modelling", Acta Metall. Mater., Vol. 42, No. 11, pp. 3817-3825, 1994.

[17] Goto, M., "Statistical Investigation of the Behaviour of Small Cracks and Fatigue Life in Carbon Steels with Different Ferrite Grain Sizes", Fat. Fract. Engng. Mater. Struct., Vol. 17, No. 6, pp. 635-649, 1994.

[18] Ishii, A., Ochi Y., Sasaki, S. K. and Nakamura, H., "Effect of Microstructure on Statistical Scatter of Crack Initiation and Growth Lives in NiCrMoV Cast Steel", J. Soc. of Mat. Sci., Japan/Zairyo, Vol. 40, No. 452, pp. 568-574, 1991.

[19] Fu-Ze, Z., "The Fatigue Scatter Factors and Reduction Factors in the Design of Aircraft and Helicopter's Structural Lives," 47th Annual Forum Proc. of the American Helicopter Society, Vol. 911984, pp. 173-178, 1991.

[20] Goto, M., "Statistical Investigation of the Behaviour of Microcracks in Carbon Steel", Fat. Fract. Engng. Mater. Struct., Vol. 14, No. 8, pp. 833-845, 1991.

[21] Sasaki, S. K., Ochi, Y., and Ishii, A., "Statistical Investigation of Surface Fatigue Cracks in Large-sized Turbine Rotor Shaft Steel", Eng. Frac. Mech., Vol. 28, No. 5/6, pp. 761-772, 1987.

[22] Dieter, G. E., *Mechanical Metallurgy*, McGraw-Hill, Third Edition, 1986.

[23] Gokhale, A. B., Rhimes, F. N., "Effect of Grain Volume Distribution on the Plastic Properties of High Purity Aluminum", *Microstructural Science*, Vol 11, Ed., DeHoff, R., Braum, J., McCall, J., Elsevier, pp. 3–11, 1983.

[24] Peterson, R. E., "Methods of Correlating Data from Fatigue Test of Stress Concentration Specimens," *Contributions to the Mechanics of Solids*, Macmillan, pp. 179-183, 1939.

[25] Fong, J. T., "Statistical Aspects of Fatigue at Microscopic, Specimen, and Component Levels," *Fatigue Mechanisms, ASTM STP 675*, pp. 729-758, 1979.

[26] Smith, R. A., "Short Fatigue Cracks", *Fatigue Mechanism: Quantitative Measurements of Physical Damage*, STP 811 Ed. Lankford, J., Davidson D. L., Morris, W. L., Wei, R. P., ASTM, pp. 264-297, 1983.

[27] Tryon, R. G., Cruse, T. A., "Probabilistic Mesomechanical Fatigue Crack Nucleation Model" Accepted for publication in ASME J. Eng. Mat. Tech., 1996.

[28] Fine, M. E. and Kwon, I. B., "Fatigue Crack Initiation Along Slip Bands", *Small Fatigue Cracks*, Ed., Ritchie, R. O. and Lankford, J., The Metallurgical Society, Warrendale, PA, pp. 29-40, 1986.

[29] Laird, C., "Mechanisms and Theories of Fatigue",*Fatigue and Microstructure*, ASM, Metals Park, Ohio, pp. 149-203, 1979.

[30] Kuhlmann-Wilsdorf, D., "Dislocation Behavior in Fatigue", Mat. Sci. Eng., Vol. 27, pp. 137-156, 1977.

[31] Forsyth, P., *The Physical Basis of Metal Fatigue*, American Elsevier Publ., New York, 1969.

[32] Brown, L. M., "Dislocation Substructure and the Initiation of Cracks by Fatigue", Metal Sci., Aug./Sept., pp. 315-320, 1977.

[33] Grobstein, L. L., Sivashankaran, S., Welsch, G., Panigrahi, N., McGervery, J. D., Blue, W., "Fatigue Damage Accumulation in Nickel Prior to Crack Initiation", Mat. Sci. Eng., Vol. A138, pp. 191-203, 1991.

[34] Tanaka, K., Mura, T., "A Dislocation Model for Fatigue Crack Initiation", ASME J. Appl. Mech., Vol. 48, pp. 97-103, 1981.

[35] Laird, C., Duquette, D. J., "Mechanisms of Fatigue Nucleation", Proceedings, Inter. Corrosion Fatigue Conference, Ed., Devereux, 0., McEvely, Steable, R. W, pp. 88-117, 1972.

[36] Laird, C., "Recent Advances in Understanding the Cyclic Deformation of Metals and Solid Solutions", *Work Hardening in Tension and Fatigue*, The Metallurgical Society, New York, pp. 150-176, 1977.

[37] Chan, K. S., Lankford, J., "A Crack Tip Strain Model for the Growth of Small Fatigue Cracks," Scripta Metall., Vol. 17, pp. 529-532, 1983.

[38] Newman, J. C., Swain, M. H., Phillips, E. P., An Assessment of the Small-Crack Effect for 2024-T3 Aluminum Alloy", *Small Fatigue Cracks*, Ed., Ritchie, R. O. and Lankford, J., The Metallurgical Society, Warrendale, PA, pp. 427-452, 1986.

[39] Grosskreutz. J. C., "The Mechanism of Metal Fatigue", Physica Status Solidi, Vol. 47b, pp 359-396, 1971.

[40] Sasaki, S., Ochi, Y., "Some Experimental Studies of Fatigue Slip Bands and Persistent Slip Bands During Fatigue Process of Low-Carbon Steel", Eng. Fract. Mech., Vol. 12, pp. 531-540, 1979.

[41] Head, A. K., and Louat, N., "The Distribution of Dislocations in Linear Arrays," Aus. J. Phys., Vol. 8, pp. 1-7, 1955.

[42] Bilby, B. A., Eshelby, J. D., "Dislocations and the Theory of Fracture," *Fracture*, Vol. 1, ed. H. Liebowitz, pp 99-182, 1968.

[43] Chang, R., Morris, W. L., Buck, O., "Fatigue Crack Nucleation at Intermetallic Particles in Alloys - A Dislocation Pile-Up Model," Scripta Metall., vol. 13, pp. 191-194, 1979.

[44] Mura, T., Tanaka, K., "Dislocation Dipole Models for Fatigue Crack Initiation", *Mechanics of Fatigue, AMD- Vol. 47*, ASME, pp. 111-132, 1981.

[45] Tanaka, K., Mura, T., "A Micromechanical Theory of Fatigue Crack Initiation from Notches," Mech. Mat., Vol. 1, pp. 63-73, 1981.

[46] Kato. M., and Mori, T., "Statistical Consideration of Fatigue Damage Accumulation", Mech. Mat., 13, pp. 155-163, 1992.

[47] Cooper, C. V., Fine, M. E., "Coffin–Manson Relation for Fatigue Crack Initiation," Scripta Metall., Vol. 18, pp. 593-595, 1984.

[48] Muskhelishvili, N. I., *Singular Integral Equations*, Noordhoff Inter., 1977.

[49] Davidson, D. L., Chan, K. S., "The Crystallography Of Fatigue Crack Initiation In Coarse Grained Astroloy At 20° C", Acta Metall., Vol. 37, No. 4, pp. 1089-1097, 1989.

[50] Mura, T., and Nakasone, Y., "A Theory of Fatigue Crack Initiation in Solids", J. Appl. Mech., 57, pp. 1-6, 1990.

[51] Venkatraman, G., Chung, Y-W., Nakasone, Y., and Mura, T., "Free Energy Formulation of Fatigue Crack Initiation Along Persistent Slip Bands: Calculation of S-N Curves and Crack Depths", Acta Metall. Mater., 38, pp. 31-40, 1990.

[52] Miller, K.J., "The Behaviour of Short Fatigue Cracks and Their Initiation. Part II–A General Summary", Fat. Frac. Eng. Mater. Struct., Vol. 10, No. 2, pp. 93-113, 1987.

[53] Davidson, D. L., "Small and Large Fatigue Cracks in Aluminum Alloys", Acta Metall., Vol. 38, No. 8, pp. 2275-2282, 1988.

[54] Hudak, S. J., Davidson, D. L., Chan, K. S., "Growth of Small Cracks in Aero Engine Disk Material", AFWAL-TR-88-4090, 1988.

[55] James, M. R., Morris, W. L., "The Effect fo Microplastic Surface Deformation on the Growth of Small Cracks",*Small Fatigue Cracks*, Ed., Ritchie, R. O. and Lankford, J., The Metallurgical Society, Warrendale, PA, pp. 145-156, 1986.

[56] Ritchie, R. O., Yu, W., "Small Crack Effects in Fatigue: A Consequence of Crack Tip Shielding", *Small Fatigue Cracks*, Ed., Ritchie, R. O. and Lankford, J., The Metallurgical Society, Warrendale, PA, pp. 167-189, 1986.

[57] Pineau A., "Short Fatigue Crack Behavior in Relationship to Three-Dimensional Aspects and Crack Closure Effect",*Small Fatigue Cracks*, Ed., Ritchie, R. O. and Lankford, J., The Metallurgical Society, Warrendale, PA, pp. 191-211, 1986.

[58] Iyyer, N. S., Dowling, N. E., "Opening and Closing of Cracks at High Cyclic Strains",*Small Fatigue Cracks*, Ed., Ritchie, R. O. and Lankford, J., The Metallurgical Society, Warrendale, PA, pp. 213-223, 1986.

[59] Brown, C., King, J., Hicks, M., "Effects of Microstructure on Long and Short Crack Growth in Nickel Based Superalloys", Met. Sci., Vol. 18, pp. 374-380, 1984.

[60] Laird,, D., Smith G. C., "Crack Propagation in High Stress Fatigue", Phil. Mag., Vol. 7 PP. 847-857, 1962.

[61] Weertman, J., "Fatigue Crack Propagation Theories", *Fatigue and Microstructure*, ASM, Metals Park, Ohio, pp. 279-206, 1979.

[62] Kikukawa, M., Jono, M., Adachi, M., "Direct Observation and Mechanics of Fatigue Crack Propagation", Proceedings of an ASTM-NBS-NSF symposium, Ed. Fong, J. T., ASTM STP 675, pp. 234-253, 1979.

[63] Hicks, M. A., Brown, C. W., "A Comparison of Short Crack Growth Behaviour in Engineering Alloys", *Fatigue 84*, Engineering Materials Advisory Services Ltd., England, pp. 1337-1347, 1984.

[64] Hudak, S. J., Chan, K. S., "In Search of a Driving Force to Characterize the Kinetics of Small Crack Growth", *Small Fatigue Cracks*, Ed., Ritchie, R. O. and Lankford, J., The Metallurgical Society, Warrendale, PA, pp. 379-406, 1986.

[65] Ewalds, H. L., Wanhill, R. J. H., *Fracture Mechanics*, Edward Arnold Publ., New York, 1991.

[66] Donahue, R. J., Clark, H. M., Atanmo, P., Kumble, R., McEvily, A. J., Inter. J. of Frac. Mech., Vol. 8, pp. 209, 1972.

[67] McEvily, A. J., *Microstructure and Design of Alloys, Vol. 2*, Inst. of Metals, pp 204, 1974.

[68] Kikukawa, M., Jono, M., Tanaka, K., "Fatigue Crack Closure Behavior at Low stress Intensity Lever", Proc. of ASM Mech. Behavior of Mat., Boston, pp. 716-720, 1976.

[69] Hobson, P. D., "The Formulation of a Crack Growth Equation for Short Cracks," Fat. Engng. Mater. Struct., Vol. 5, pp. 323-327, 1982.

[70] Chan, K. S., Lankford, J. "The Role of Microstructural Dissimilitude in Fatigue and Fracture of Small Cracks," Acta Metall., Vol. 36, No. 1, pp.193-206, 1988.

[71] W. W. Gerberich and N. R. Moody, "A Review of Fatigue Fracture Topology Effects on Threshold and Growth Mechanisms," *Fatigue Mechanisms, ASTM STP 675*, pp. 292-341, 1979.

[72] Bilby, B. A., Cottrell, A. H., Swinden, K. H., "The Spread of Plastic Yield from a Notch," Proc. Roy. Soc., Vol. A272, pp. 304-314, 1963.

[73] Dugdale, D. S., "Yielding of Steel Sheets Containing Slits," J. Mech. Phys. Sol., Vol. 8, pp.100-104, 1960.

[74] Weertman, J., "Rate of Growth of Fatigue Cracks Calculations from the Theory of Infinitesimal Dislocations Distributed on a Plane," J. Frac. Mechs., Vol. 2, pp. 460-467, 1966.

[75] Weertman, J., "Crack Tip Stress Intensity Factor of the Double Slip Plane Crack Model: Short Cracks and Short Short-cracks," Int. J. Frac., Vol. 26, pp. 31-42, 1984.

[76] Taira, S., Tanaka, K., Nakai, Y., "A Model of Crack Tip Slip Band Blocked by Grain Boundary," Mech. Res. Comm., Vol. 5, No. 6, pp. 375–381, 1978.

[77] Tanaka, K., Akiniwa, Y., Nakia, Y., Wei, R. P., "Modeling of Small Fatigue Crack Growth Interacting with Grain Boundary," Engng. Frac. Mechs., Vol. 24, No. 6, pp. 803–819, 1986.

[78] Morris, W. L., James, M. R.,, Buck, O., "A Simple Model of Stress Intensity Range Threshold and Crack Closure Stress," Engng. Frac. Mechs., Vol. 18, pp. 871-877, 1983.

[79] de los Rios, E. R., Tang, Z., Miller,K. J., "Short Crack Fatigue Behavior in a Medium Carbon Steel," Fat. Engng. Mat. Struct., Vol. 7, pp. 97-108, 1984.

[80] Navarro, A., de los Rios, E. R., "A Microstructurally Short Fatigue Crack Growth Equation," Fat. Frac. Engng. Mater. Struct., Vol. 11, No. 5, pp. 383-396, 1988.

[81] Newby, M. J., "Markov Models for Fatigue Crack Growth", Eng. Frac. Mech., Vol. 27, No. 4, pp. 477-482, 1987.

[82] Yang, J. N., Salivar, G. C., Annis, C. G., *Statistics of Crack Growth in Engine Materials - Volume 1: Constant Amplitude Fatigue Crack Growth at Elevated Temperatures*, AFWAL-TR-82-4040, 1982.

[83] W. L. Morris, M. R. James, and O. Buck, "Computer Simulation of Fatigue Crack Initiation," Engng. Frac. Mechs., Vol. 13, pp. 213–221, 1980.

[84] Tanaka K., Kinefuchi, M., and Yokomaku, T., "Modelling of Statistical Characteristics of the Propagation of Small Fatigue Cracks", *Short Fatigue Cracks*, Eds. Miller, K. J., and de los Rios, E. R., ESIS 13, Mechanical Engineering Publications, London, pp. 351-368, 1992.

[85] Cox, B. N., Pardee W. J., Morris, W. J., "A Statistical Model of Intermittent Short Fatigue Crack Growth", Fat. Frac. Engng. Mater. Struct., Vol. 9, No. 6, pp. 435-455, 1987.

[86] Bruckner-Foit, A., Jackels, H., Lahodny, H., Munz, D., "Fatigue Reliability of Components Containing Microstructural Flaws", Proceedings of ICOSSAR '89, pp. 1499-1506, 1989.

[87] Kitamura, T., Ohtani, R., "Creep Life Prediction Based on Stochastic Model of Microstructurally Short Crack Growth", ASME J. Engng. Mat. Tech., Vol. 111 pp. 169-175, 1989.

[88] Sun, Z., de los Rios, E. R., Miller, K. J., "Modelling Small fatigue Cracks Interacting with Grain Boundaries", Fat. Frac. Engng. Mater. Struct., Vol 14. No. 2/3, pp. 277-291, 1991.

[89] Smith, C. S., *A Search for Structure*, MIT Press, Cambridge, 1981.

[90] Kurtz, S. K., Carpay, F. M. A., "Microstructure and Normal Grain Growth in Metals and Ceramics. Part I. Theory", J. Appl. Phys., Vol. 51, No. 11, pp. 5725-5744, 1980.

[91] Kumar, S., Kurtz, S. K., Banavar, J. R., and Sharma, M. G., "Properties of a Three-Dimensional Poisson-Voronoi Tessellation: A Monte Carlo Study.", J. of Stat. Phys., Vol. 67, Nos. 3/4, pp. 523-551, 1992.

[92] Ang, A. H.-S., Tang, W.H., *Probability Concepts in Engineering Planning and Design*, Vol 1, John Wiley and Sons, New York, 1975.

[93] Barenblatt, G. I., "On a Model of Small Fatigue Cracks", Eng. Frac. Mech., Vol. 28, No. 5/6, pp. 623-626, 1987.

[94] Kozaczek, K. J., Petrovic, G. B., Ruud, C. O., and McIlree, A. R., "Modeling of Stress Distributions on the Microstructural Level in Alloy 600", *Fatigue and Crack Growth: Environmental Effects, Modeling Studies, and Design Considerations*, PVP-Vol. 306, ASME, pp. 223-232, 1995.

[95] Schimd, E., Z. Eledtrodhem., Vol. 37, pp. 447, 1931.

[96] Tanaka, T., Kosugi, M., "Crystallographic Study of the Fatigue Crack Nucleation Mechanism in Pure Iron", *Basic Questions in Fatigue, Vol. 1*, ASTM STP 924, pp. 98-119, 1988.

[97] Barrett, C. S., *Structure Of Metals*, McGraw-Hill Book Company, Inc., Second edition, 1952.

[98] Backofen, W. A., *Deformation Processing*, Addison-Wesley, pp. 72-82, 1972.

[99] Taylor, G. I., "Plastic Deformation in Metals", J. Inst. Metals, Vol. 62, pp. 307-24, 1938.

[100] Bishop, J. F. W., Hill, R., Phil. Mag., Vol. 42, pp. 1298-1307, 1951.

[101] Hosoford Jr., W. S., Backofen, W. A., "Strength and Plasticity of Textured Metals", *Fundamentals of Deformation Processing*, Ed., Backofen W. A., Burke, J. J., Coffin Jr., L. F., Weiss, V., Syracuse University Press, pp. 259-297, 1964.

[102] Chin, G. Y., Mammel, W. L., "Computer Solution of the Taylor Analysis for Axisymmetric Flow", Trans. Metall. Soc., Vol. 239, pp. 1400-1405, 1967.

[103] de los Rios, E. R., Navarro, A., "Considerations of Grain Orientation and Work Hardening on Short-Fatigue-Crack Modelling", Phil. Mag. A, Vol. 16, No. 3, pp. 435-449, 1990.

[104] de los Rios, E. R., Xin, X. J., Navarro, A., "Modelling Microstructurally Sensitive Fatigue Small Crack Growth", Proc. Roy. Soc. A, Vol. 447, No. 1929, pp. 111-134, 1994.

[105] Armstrong, R., Codd, I., Douthwaite, R. W., Petch, N. J., "The Plastic Deformation of Polycrystalline Aggregates", Phil. Mag., Vol. 7, pp. 45-58, 1962.

[106] Armstrong, R. W., "The Strengthening or Weakening of Polycrystals Due to the Presence of Grain Boundaries", Canadian Metall. Quart., Vol. 13, No. 1, pp. 187-202, 1974.

[107] Chudnovsky, A., and Kunin, B., "A Probabilistic Model of Brittle Crack Formation", J. Appl. Phys., Vol. 62, No. 10, pp. 4124-4129, 1987.

[108] Mull, M. A., and Chudnovsky, A., "A Probabilistic Approach to the Fracture Toughness of Composites", Phil. Mag. A, Vol. 56, No. 3, pp. 419-443, 1987.

[109] Moet, A., Mostafa, I., Chudnovsky, A., and Kunin, B., "Probabilistic Fracture Mechanics of 2D Carbon-Carbon Composites", Inter. J. Frac., 55, pp. 179-191, 1992.

[110] Char, B. W., Geddes K.O., Gonnet, G.H., Leong, B.L., Monagan, M.B., Watt, S. W., *Maple V. First Leaves*, Springer-Verlag, New York, 1992.

[111] Tryon, R. G., Cruse, T. A., "A Reliability-Based Model to Predict Scatter in Fatigue Crack Nucleation Life", Submitted to Fat. Frac. Eng. Mat. Str., 1996.

[112] Phillips, E. P., Newman, J. C., "Impact of Small-Crack Effects on Design-Life Calculations", Experimental Mech., Vol. 29, No. 2, pp. 221-225, 1989.

[113] Gerdes, C., Gyser, A., Lutjering, G., "Propagation of Small Surface Cracks in Ti-Alloys", *Fatigue Crack Growth Threshold Concepts*, Ed. Davidson, D. L., Suresh, S., AIME, Warrendale, PA., pp. 465-478, 1984.

[114] Brown, C. W., King, J. E., "The relevance of microstructural Influenced in the Short Crack Regime to Overall Fatigue Resistance", *Small Fatigue Cracks*, Ed., Ritchie, R. O. and Lankford, J., The Metallurgical Society, Warrendale, PA, pp. 73-95, 1986.

[115] Gayda, J., Miner, R. V., "The Effect of Microstructure on 650C Fatigue Crack Growth in P/M Astroloy", Metall. Trans. A, Vol 14A, pp. 2301-2308, 1983.

[116] Lerch B. A., Jayaraman, K., Antolovich, S. D., "A Study of Fatigue Damage Mechanisms in Waspaloy for 25 to 800C", Mat. Sci. Eng., Vol. 66, pp. 151-166, 1984.

[117] Tokaji, K., Ogawa, T., "The Growth Behaviour of Microstructurally Small Fatigue Cracks in Metals",*Short Fatigue Cracks*, Eds. Miller, K. J., and de los Rios, E. R., ESIS 13, Mechanical Engineering Publications, London, pp. 85-99, 1992.

[118] Reed, P. A., King, J. E., "Comparison of Long and Short Crack Growth in Polycrystalline and Single Crystal Forms of Udimet 720",*Short Fatigue Cracks*, Eds. Miller, K. J., and de los Rios, E. R., ESIS 13, Mechanical Engineering Publications, London, pp. 153-168, 1992.

[119] Weiss, B., Stickler, R., Fathulla, A., "Initiation and Transition of Short to Long Fatigue Cracks in Technical Alloys", *Small Fatigue Cracks*, Ed., Ritchie, R. O. and Lankford, J., The Metallurgical Society, Warrendale, PA, pp. 471-497, 1986.

[120] Larsen, J. M., Nicholas, T., Thompson, A. W., Williams, J. C., "Small Crack Growth in Titanium-Aluminum Alloys", *Small Fatigue Cracks*, Ed., Ritchie, R. O. and Lankford, J., The Metallurgical Society, Warrendale, PA, pp. 499-512, 1986.

[121] Nishijima, S., Masuda, C., Abe, T., Ohta, Y., Tackeuchi, E., Komatsu, A., Ishii, A., Matsuyama, T., Sumiyoshi, T., "Evaluation of Statistical Fatigue Properties and their Heat-to Heat Variations of S25C, S45C, and SCM3 Steels", Trans. Natnl. Res. Inst. Met., Vol. 19, No. 3, pp. 33-46, 1977.

[122] Nishijima, S., Masuda, C., Abe, Komatsu, A.,Ishii, A., Matsuyama, T., Sumiyoshi, T., Tanaka, Y., Otsubo, S., "Statistical Fatigue Properties of Heat Treated JIS Steels, S45C, SCM3, SNCM8, SK5, and SUS403, for Machine Use",Trans. Natnl. Res. Inst. Met., Vol. 19, No. 6, pp. 43-59, 1977.

[123] Weibull, W., *Fatigue Testing and Analysis of Results*, Pergamon Press, 1961.

[124] Trantina, G., "Statistical Fatigue Failure Analysis", J. of Test. Eval., Vol. 9, No. 1, pp. 44-49, 1981.

[125] Rhimes, F. N., Patterson, B. R., "Effect of the Degree of Prior Cold Work on the Grain Volume Distribution and the Rate of Grain Growth of Recrystallized Aluminum", Metall. Trans. A, Vol. 13A, pp. 985-993, 1982.

[126] Bailon, J-P., Antolovich, D., "Effect of Microstructure on Fatigue Crack Propagation: a Review of Existing Models and Suggestions for Further Research", *Fatigue Mechanism: Quantitative Measurements of Physical Damage*, STP 811 Ed. Lankford, J., Davidson D. L., Morris, W. L., Wei, R. P., ASTM, pp. 313-349, 1983.

[127] Davidson, D. L., Lankford, J., "High Resolution Techniques fo the Study of Small Cracks", *Small Fatigue Cracks*, Ed., Ritchie, R. O. and Lankford, J., The Metallurgical Society, Warrendale, PA, pp. 455-470, 1986.

[128] Bucci, R. J., Brazill, R. L., Brockengrough, J. R., "Assessing Growth of Small Flaws from Residual Strength Data", *Small Fatigue Cracks*, Ed., Ritchie, R. O. and Lankford, J., The Metallurgical Society, Warrendale, PA, pp. 541-556, 1986.

[129] Jenkins, P. J., Briggs, G. A. D., "The Measurement of Surface Cracks Using Acoustic Microscopy", *Short Fatigue Cracks*, Eds. Miller, K. J., and de los Rios, E. R., ESIS 13, Mechanical Engineering Publications, London, pp. 321-334, 1992.

[130] Stephens, R., Grabowski, L., Hoeppner, D. W., "In-Situ/SEM Fatigue Studies of Short Crack Behaviour at Ambient and Elevated Temperature in a Nickel-Based Superalloy",*Short Fatigue Cracks*, Eds. Miller, K. J., and de los Rios, E. R., ESIS 13, Mechanical Engineering Publications, London, pp. 335-348, 1992.

[131] Vanmarcke, E., Grigoriu, M., "Stochastic Finite Element Analysis of Simple Beams", J. Engng. Mech., ASCE, Vol. 109, No. 5, pp. 1203-1214, 1983.

[132] Mahadevan, S., Haldar, A., "Practical Random Field Discretization in Stochastic Finite Element Analysis", Structural Safety, Vol. 9, pp. 283-304, 1991.

[133] Ashbaugh, N.E., Khobaib, M., John, R.,"Mechanical Properties for Advanced Engine Materials," AFRWL-TR-91-4149, 1992.

REPORT DOCUMENTATION PAGE

Form Approved
OMB No. 0704-0188

1. AGENCY USE ONLY (*Leave blank*)	2. REPORT DATE	3. REPORT TYPE AND DATES COVERED
	April 1997	Final Contractor Report

4. TITLE AND SUBTITLE

Probabilistic Mesomechanical Fatigue Model

5. FUNDING NUMBERS

WU-523-22-13
G-NGT-51053

6. AUTHOR(S)

Robert G. Tryon

7. PERFORMING ORGANIZATION NAME(S) AND ADDRESS(ES)

Vanderbilt University
Nashville, Tennessee 37203

8. PERFORMING ORGANIZATION REPORT NUMBER

E-10727

9. SPONSORING/MONITORING AGENCY NAME(S) AND ADDRESS(ES)

National Aeronautics and Space Administration
Lewis Research Center
Cleveland, Ohio 44135-3191

10. SPONSORING/MONITORING AGENCY REPORT NUMBER

NASA CR-202342

11. SUPPLEMENTARY NOTES

Project Manager, Christos C.Chamis, Technology Directorate, NASA Lewis Research Center, organization code 5000, (216) 433-3252.

12a. DISTRIBUTION/AVAILABILITY STATEMENT

Unclassified - Unlimited
Subject Category 39

This publication is available from the NASA Center for AeroSpace Information, (301) 621-0390.

12b. DISTRIBUTION CODE

13. ABSTRACT (*Maximum 200 words*)

A probabilistic mesomechanical fatigue life model is proposed to link the microstructural material heterogeneities to the statistical scatter in the macrostructural response. The macrostructure is modeled as an ensemble of microelements. Cracks nucleat within the microelements and grow from the microelements to final fracture. Variations of the microelement properties are defined using statistical parameters. A micromechanical slip band decohesion model is used to determine the crack nucleation life and size. A crack tip opening displacement model is used to determine the small crack growth life and size. Paris law is used to determine the long crack growth life. The models are combined in a Monte Carlo simulation to determine the statistical distribution of total fatigue life for the macrostructure. The modeled response is compared to trends in experimental observations from the literature.

14. SUBJECT TERMS	15. NUMBER OF PAGES
Fatigue scatter; Damage accumulation, Crack nucleation; Fast fracture; Probabilistic mesomechanics; Material microstructure; Cycle loads; Monte Carlo simulation	109
	16. PRICE CODE A06

17. SECURITY CLASSIFICATION OF REPORT	18. SECURITY CLASSIFICATION OF THIS PAGE	19. SECURITY CLASSIFICATION OF ABSTRACT	20. LIMITATION OF ABSTRACT
Unclassified	Unclassified	Unclassified	